Nuclear Physics A531 (1991) 709–745
North-Holland

A REEXAMINATION OF THE ABRASION–ABLATION MODEL FOR THE DESCRIPTION OF THE NUCLEAR FRAGMENTATION REACTION*

J.-J. GAIMARD[1] and K.-H. SCHMIDT

Gesellschaft für Schwerionenforschung, 6100 Darmstadt, Postfach 110552, Germany

Received 12 November 1990
(Revised 18 February 1991)

Abstract: The nuclear fragmentation reaction is studied as an important production mechanism for secondary beams. The geometrical abrasion model and a macroscopic evaporation model which describe the two steps of the reaction are reexamined. Several improvements and modifications of these models are discussed and a new model description incorporating these elements is proposed. In particular, the excitation energy and the angular-momentum distribution of the prefragments, the formulation of evaporation as a diffusion process and the role of microscopic structure in the production cross section are considered. The new model description preserves the simplicity and the transparency of the original models. The predictions of the new model are compared to those of the original models and to experimental cross sections. While the original models showed several systematic discrepancies in comparison to measured cross sections, the new model is able to reproduce the whole body of experimental data with satisfactory agreement.

1. Introduction

The formation of projectile-like or target-like fragmentation products in peripheral heavy-ion collisions at relativistic energies has been studied theoretically already many years ago with much success by use of microscopic [1]) as well as macroscopic model descriptions [2]). Since then several attempts have been made to improve the understanding of the fragmentation process. However, the detailed explanation of some aspects of the observed phenomena is still in an unsatisfactory state. That is why much effort has been invested to develop empirical systematics, e.g. refs. [3,4]), in order to allow reliable estimations of fragmentation cross sections. The recent increase of experimental data on fragmentation reactions and, moreover, the better knowledge on nuclear properties, concerning e.g. nuclear dynamics and nuclear level densities, gave the motivation to make a new effort for a detailed understanding of the fragmentation process which will be presented in this paper. It is the aim of this investigation to enable a reliable prediction of fragmentation cross sections for certain isotopes in order to estimate the intensity of secondary radioactive beams which are becoming available at several experimental facilities.

According to a proposition of Serber [5]) inelastic nuclear reactions at relativistic energies can be described in two steps which occur in two distinctly different time

* This work forms a part of the Ph.D. thesis of J.-J. Gaimard, Université Paris 7, 1990.

[1] Present address: Inst. f. Kernphysik THD, 6100 Darmstadt, Schlossgartenstr. 9, Germany.

scales. The first spontaneous interaction may modify the composition of the reaction partners and introduces a certain amount of excitation energy. The characteristic time of this reaction step is several times 10^{-23} s. In the second reaction step the system reorganizes, that means it thermalizes and deexcites by the evaporation of neutrons, protons and light nuclei as well as by fission and emission of gamma rays. During the whole deexcitation phase there is a competition between these different processes. According to the statistical model the characteristic time for the emission of particles varies between $\sim 10^{-16}$ s at an excitation energy of 10 MeV and $\sim 10^{-21}$ s at 200 MeV.

The different reaction types may be classified according to the impact parameter. A typical process for peripheral collisions is the fragmentation reaction in which one or several nucleons are removed in the spontaneous interaction and several others are evaporated in the deexcitation phase. The observation of higher multiplicities of relatively heavy products has been attributed to a complex break-up process, the multifragmentation which is expected to occur in more central collisions where higher compression values and nuclear temperatures are reached [6-10]). However, Friedman *et al.* [11,12]) and Moretto *et al.* [13]) stress that at least part of these observations might also be explained by sequential fission of fragmentation products. In the present work we rather restrict ourselves to peripheral collisions leading to a single prefragment per reaction partner.

There are several models which describe the first step of the fragmentation process. Some of the mostly used models are the intranuclear-cascade model [1]) and the abrasion model [2]). The intranuclear-cascade model relies on a microscopic description. The nuclear reaction is treated as a series of individual nucleon-nucleon interactions. The most recent versions [14,15]) of this model consist of calculations of the type Boltzmann, Uehling, Uhlenbeck (BUU) or Vlasov, Uehling, Uhlenbeck (VUU) and incorporate a self-consistent mean field as well as the Pauli blocking. The abrasion model is a macroscopic description. It relies on the picture of a clean cut of the target nucleus by the projectile and *vice versa*. The geometrical abrasion model expresses well the main features of peripheral high-energetic nucleus-nucleus collisions. If the relative velocity of the reaction partners is higher than the Fermi velocity of the nucleons, nucleon-nucleon collisions are mostly restricted to the overlap zone, whereas the spectators, e.g. the parts of projectile and target outside the overlap zone, continue to move almost with the initial velocities of projectile and target. This geometrical model has been justified using Glauber-type calculations [16]) by Hüfner *et al.* [17]).

The second stage of the fragmentation process is generally treated in a more or less sophisticated way by numerical statistical-model codes. A much more elegant and transparent formulation of the statistical model was proposed by Campi and Hüfner who treated this ablation stage in a macroscopic way on the basis of a master equation which lead them to a diffusion equation [18]). The evaporation stage is also the final process of other reaction types like e.g. the multifragmentation.

Therefore the models for fragmentation and multifragmentation deal with many similar problems.

In the present paper, we will critically discuss the two macroscopic models describing the fragmentation reaction in some detail. In particular, we will propose a few modifications which remove some inconsistencies and shortcomings while the simplicity of the original models is preserved. Finally, the predictions of the modified models will be compared to the body of the available experimental data.

2. A reminder on macroscopic nuclear fragmentation models

In the following sections we will briefly remind on the abrasion model and the evaporation model of Campi and Hüfner. This will give us a basis for a reexamination of our understanding of the fragmentation process.

2.1. THE ABRASION STAGE

The abrasion model considers a geometrically defined separation in an overlap or "participator" zone where nucleons of projectile and target interact and finally form a hot fireball [19]) or firestreak [20]) as well as the non-overlapping "spectator" zones named prefragments where part of the nucleons of projectile and target keep on moving almost undisturbed with their initial velocities. In the following we will consider projectile fragmentation only, but it is evident that the physics of the target fragmentation is identical if the reference frames are interchanged.

The formulation of the abrasion model is described in refs. [2,21,22]). For a specific projectile-target combination, the number of nucleons removed from the projectile only depends on the impact parameter. It can be calculated by a numerical integration of the overlap volume. There also exists an approximate analytical formula proposed by Swiatecki [23,24]) which has been shown by Morrissey *et al.* [21]) to be a good approximation for large impact parameters. In this way the mass number of the projectile prefragment is determined by the impact parameter as well as its production cross section. The cylindrical cut of the spherical projectile provokes the rupture of a certain number of nucleon-nucleon bindings. In the geometrical concept of the abrasion model, the excitation energy of the prefragment is given by the excess of the surface of the deformed prefragment with respect to a sphere of equal volume. It can be calculated numerically or by the analytical approximation of Swiatecki [23,24]). This description can be improved by using more realistic nuclear-matter distributions [25]) deduced from the droplet model [26]) including the diffuseness.

Although the results of the abrasion-ablation model agree generally well with the experimental data, they show some systematic deviations. These deviations are attributed to an underestimated excitation energy of the prefragments. Thus, another mechanism creating an additional amount of excitation energy was proposed, consisting of nucleons of the abrasion zone penetrating the prefragments and

deposing part of their kinetic energy by scattering [17,22]). There exist several versions of the abrasion model which include a frictional energy (e.g. refs. [17,22,28])). They are usually known as extended abrasion models.

The abrasion process described above determines only the number of nucleons removed from the initial nucleus and does not specify its proton-to-neutron ratio. We will mention a few different methods applied for this task. The first, used in ref. [19]), supposes that the proton-to-neutron ratio of the projectile prefragment is exactly that of the initial projectile nucleus, that means this model corresponds to a situation where the removed protons and neutrons are completely correlated. The second way to calculate the charge distribution of the prefragments consists in assuming that every nucleon removed has a statistical chance to be a neutron or a proton as determined by the neutron-to-proton ratio of the precursor nucleus. With this hypothesis, the isobaric cross section $\sigma(A', Z')$ of the projectile prefragment is linked to the mass cross section $\sigma(A')$ in the following way:

$$\sigma(A', Z') = \frac{\binom{Z_p}{z}\binom{N_p}{n}}{\binom{A_p}{a}} \sigma(A'), \tag{2.1}$$

where Z_p, N_p and A_p are the numbers of protons, neutrons, and nucleons, respectively, from the initial projectile, while z, n and a are the corresponding quantities of the particles removed from the projectile by the abrasion. This hypergeometrical model corresponds to the extreme situation of no correlation at all between the nucleons during the abrasion and results in the largest charge distribution width obtainable. The third way to calculate the charge distribution of the prefragment was proposed by Morrissey *et al.* [21]). They suppose that the fluctuation of the proton-to-neutron ratio of the nucleus removed from the projectile is governed by the zero-point oscillation of the giant dipole resonance (GDR). This model corresponds to an intermediate situation between the two preceding cases. Besides this, there exist several other models which describe the nuclear proton–neutron correlation, e.g. the hydrodynamical model of Bondorf *et al.* [27]).

2.2. THE EVAPORATION STAGE

After the first reaction step, the prefragments may be considered as an ensemble classified by a few macroscopic variables. These are the mass number A', the neutron excess I', defined as the difference of the number of neutrons and protons of the nucleus, and the excitation energy E'. According to ref. [18]), the evolution of the evaporation process is described by the following master equation:

$$\frac{dP}{dt}(\underset{\sim}{x}; t) = -P(\underset{\sim}{x}; t) \int M(\underset{\sim}{x} \to \underset{\sim}{y}) \Omega(\underset{\sim}{y})\, d\underset{\sim}{y} + \int P(\underset{\sim}{y}; t) M(\underset{\sim}{y} \to \underset{\sim}{x}) \Omega(\underset{\sim}{x})\, d\underset{\sim}{y}, \tag{2.2}$$

whereby P is the probability to find the system in a state $\underset{\sim}{x}$ characterized by (A, E, I) at the time t, $\Omega(\underset{\sim}{x})$ being the density of states. The matrix $M(\underset{\sim}{x} \to \underset{\sim}{y})$ describes the transition from the state $\underset{\sim}{x}$ to a modified state $\underset{\sim}{y}$. At the end of the process $(t \to \infty)$ the final fragments are formed.

For the determination of the matrix $M(\underset{\sim}{x} \to \underset{\sim}{y})$ the authors restrict themselves to the evaporation of neutrons, protons and alpha particles. The statistical weights are deduced from their intrinsic spin and thus they arrive at the values $\frac{2}{5}$, $\frac{2}{5}$ and $\frac{1}{5}$ for the neutron, proton and alpha particle, respectively. The mean number of nucleons emitted in one evaporation step is:

$$\alpha = \langle \Delta A \rangle = \tfrac{2}{5} \cdot 1 + \tfrac{2}{5} \cdot 1 + \tfrac{1}{5} \cdot 4 = \tfrac{8}{5}. \tag{2.3}$$

The mean exchanged neutron excess is $\tau_1 = \langle \Delta I \rangle = 0$ and its mean quadratic value

$$\tau_2 = \langle (\Delta I - \langle \Delta I \rangle)^2 \rangle = \tfrac{2}{5} \cdot 1 + \tfrac{2}{5} \cdot 1 + 0 = \tfrac{4}{5}. \tag{2.4}$$

The mean reduction of excitation energy per evaporation step was estimated to be $e = 20$ MeV.

The evaporation chain stops if the excitation energy falls below the lowest particle threshold of the residual nucleus. The length of the evaporation chain links the mass-production cross section $\sigma(A)$ of the final fragment to the formation cross section of the prefragment. At the end of the evaporation, the isobaric cross section $\sigma(A, I)$ for a fixed mass number A is described by:

$$\sigma(A, I) = c(A) \frac{\Omega(A, I, E_t(A, I))}{\Omega(A, I_S, E_t(A, I_S))} \left[\exp \frac{-(I - I')^2}{2\tau_2(A' - A)/\alpha} \right] \sigma(A), \tag{2.5}$$

where $c(A)$ is a normalization constant and $\Omega(A, I, E_t)$ the state density of the fragment characterized by A and I at the lowest threshold energy $E_t(A, I)$. This state density is normalized to that of the most-bound isobar ($I = I_S$). The state-density factor in eq. (2.5) is the equilibrium term. It defines the neutron-to-proton ratio of fragments after a long evaporation chain, that means it defines the equilibrium-residue corridor. The gaussian term may be called memory factor. This term is the solution of a diffusion equation deduced from the master eq. (2.2). It describes the influence of the projectile on the neutron-to-proton ratio of the fragments.

3. A few modifications to the model description of the nuclear fragmentation process

The models presented in the preceding chapters for the two steps of the fragmentation reaction can be combined in order to obtain a simple and transparent model description for the nuclear fragmentation reaction. However, before doing so we will discuss some inconsistencies and shortcomings of the existing models and propose a few modifications.

The first subject of criticism concerns the evaluation of the excitation energy in the abrasion model based on the excess of surface energy. We will develop an

alternative model description of the excitation energy which turns out to give larger values and tends to solve part of the difficulties connected with the underestimation of the excitation energy by the original description. In analogy to the Goldhaber description of the momentum width induced by the fragmentation we will estimate the angular-momentum distribution of the prefragments. Another modification concerns some approximations of the evaporation model of Campi and Hüfner. In particular, the evaporation of only one representative average particle without considering the influence of the residual states in each evaporation step on the competition between the different kinds of evaporated particles seems to us a bit too crude. We will propose some modifications to this evaporation model which tend to give more realistic results. In a further detailed discussion we will analyze the influence of microscopic effects in the state densities on the fragmentation yields.

3.1. THE ENERGY OF THE PREFRAGMENTS DUE TO THE CREATION OF VACANCIES IN THE FERMI DISTRIBUTION

While the abrasion model [2]) seems to us suitable to estimate the number of nucleons removed from the projectile [17]), it seems to us inappropriate to take the excess of surface energy as a measure of the excitation energy induced by the rupture of the nucleon–nucleon bindings. When the reaction partners approach each other in their ground state, the nucleons move in the appropriate nuclear potential well with their Fermi velocity, whereby their mean free path is large compared to the size of the nuclei. At relativistic energies, the projectile velocity is large compared to the Fermi velocity. Therefore, the chance to remove a certain nucleon in a peripheral collision is given by the probability to find it at the instant of the reaction in the overlap zone. Thus, the total number of nucleons removed is proportional to the volume of the overlap zone. The wave functions of the remaining nucleons are only little disturbed by the abrasion; in particular they are not expected to adapt themselves to a specific deformation. In this diabatic picture, the prefragment keeps the same geometrical extension as the original nucleus with a reduced density. In the contrary, the original abrasion model is valid for a classical liquid with a short mean free path of the constituents. If applied to nuclei it would suggest that the nucleons in the prefragments after the abrasion occupy the energetically most favorable orbits which fit best to their shapes as generated by the geometrical cut. However, this would require an adiabatic process which is *a priori* not justified.

We propose the following approach for calculating the excitation energy of the prefragment: The nucleons are bound in the potential well of the nucleus. During the abrasion, the orbits of the nucleons not removed are preserved. This is suggested by the short time span of the abrasion, in the order of $(2\text{–}5) \times 10^{-23}$ s. By the abrasion, a certain number of single-particle levels is vacated, and the excitation energy is given by the sum of the energies of these holes with respect to the Fermi surface. For a quantitative estimate we take a Woods–Saxon potential with an average depth

of −47.4 MeV for neutrons and protons [29]). We neglect that the density reduction caused by the abrasion decreases the potential depth because it is reestablished after the contraction to normal nuclear density. The energy generated by one hole varies between 0 and 40 MeV depending on its position if we assume a Fermi energy around −7.4 MeV. In order to calculate the mean energy induced by one hole in the potential well below the Fermi surface, we use the single-particle level density $g(\varepsilon)$ of the Woods-Saxon potential which can be described approximately by $g \sim \varepsilon$ [ref. [30])] if ε is the single-particle energy counted from the bottom of the potential well, and we assume that the probability for generating the hole is the same for each level. This statistical hole-energy model gives an average excitation energy of 13.3 MeV per hole.

In the following we will investigate whether the basic assumption of our proposed model is justified, namely that the orbits of the nucleons of the prefragment are untouched by the abrasion process, that means whether the abrasion process at relativistic energies is diabatic. For this purpose we will estimate the part of the excitation energy which is thermalized during the abrasion, that means the part which is equilibrated and modifies the orbits of the nucleons of the prefragment. According to calculations of Bertsch [31]), Nörenberg [32]) estimated an intrinsic thermalization time, also called intrinsic equilibration time, by the following relation:

$$\tau_{\text{intr}}(t) = 2 \times 10^{-22}\,\text{MeV} \cdot \text{s}/e^*(t)\,, \tag{3.1}$$

with e^* being the excitation energy per nucleon of the system as a function of time t. In order to simplify the calculation we suppose for the peripheral collisions that the excitation energy deposited in the prefragment during the abrasion process is linear as a function of time:

$$e^*(t) = C_1 t, \qquad \text{for } 0 \leqslant t \leqslant t_1\,, \tag{3.2}$$

with

$$C_1 = E'/A' t_1\,, \tag{3.3}$$

whereby E' and A' are the total excitation energy and the mass of the prefragment, respectively, after the abrasion, and t_1 is the abrasion time. During the abrasion process, the variation of the excitation energy per nucleon which is not thermalized is given by:

$$\frac{\mathrm{d}e}{\mathrm{d}t} = C_1 - \frac{e}{\tau_{\text{intr}}}\,.$$

By integration we obtain at the end of the abrasion process:

$$e(t) = C_1 \left(\int_0^t \exp\left[0.5 C_2 t'^2\right] \mathrm{d}t' \right) \exp\left[-0.5 C_2 t^2\right], \tag{3.4}$$

with

$$C_2 = \frac{1}{2 \times 10^{-22}\,\text{MeV} \cdot \text{s}} \frac{E'}{A' t_1}\,. \tag{3.5}$$

In table 1 we present the results of our calculation for different systems. The total excitation energy per nucleon e^* deposited in the prefragment is calculated according to the statistical hole-energy model, and the number of nucleons removed from the projectile is calculated by the abrasion model. The abrasion time is given by geometrical considerations. The numbers show that the fraction of the excitation energy which is thermalized in the prefragment during the abrasion process is quite small for peripheral collisions at relativistic energies. This result justifies the validity of the statistical hole-energy model: The abrasion process is an almost diabatic process which hardly modifies the orbits of the nucleons in the prefragment.

Several corrections could be applied to the proposed model for the excitation energy of the prefragment; e.g. the displacement of the center of mass [17]) and the position distributions of the nucleons in the different orbits. However, we are convinced that the present formulation gives already a good estimate of the excitation energy induced by the fragmentation process if final-state interactions between the firestreak and the spectator zones are not considered. Since the actual formulation of the final-state interaction is primarily motivated by the shortcoming of the surface-energy model, we will not include it and try to determine the importance of additional friction effects by comparing the predictions of our new model with experimental data.

Fig. 1 shows the average excitation energy as a function of the prefragment for the two systems: $^{48}Ca+^{9}Be$ and $^{209}Bi+^{12}C$. The predictions of the statistical hole-energy model are compared to those of the original abrasion model [2]) and an extended version including a frictional energy [28]). The excitation energy of the prefragments calculated with the proposed model lies between those of the original and the extended models if less than four nucleons are removed and agrees well to the values of the extended model for more central collisions.

The proposed statistical hole-energy model predicts a rather broad excitation-energy distribution. This distribution is linear in energy in the case of only one removed nucleon as it depends on the single-particle state density $g \sim \varepsilon$. The energy

TABLE 1

Calculated fraction of energy which is equilibrated during the abrasion process for four different systems

Projectile (energy) + target	A'	t_1 (s)	$e^*(t_1)$ (MeV/u)	$e(t_1)$ (MeV/u)	f (%)
^{48}Ca (1 GeV/u) + ^{9}Be	46	2.9×10^{-23}	0.578	0.562	2.7
^{48}Ca (1 GeV/u) + ^{9}Be	38	3.9×10^{-23}	3.495	2.799	19.9
^{100}Mo (1 GeV/u) + ^{12}C	98	3.2×10^{-23}	0.270	0.266	1.4
^{100}Mo (1 GeV/u) + ^{12}C	90	4.5×10^{-23}	1.481	1.327	10.4

A' is the mass of the projectile prefragment, t_1 the abrasion time, $e^*(t_1)$ the excitation energy per nucleon introduced in the prefragment due to the abrasion, $e(t_1)$ the excitation energy per nucleon not thermalized just at the end of the abrasion process and f the fraction of the energy which is thermalized during the abrasion.

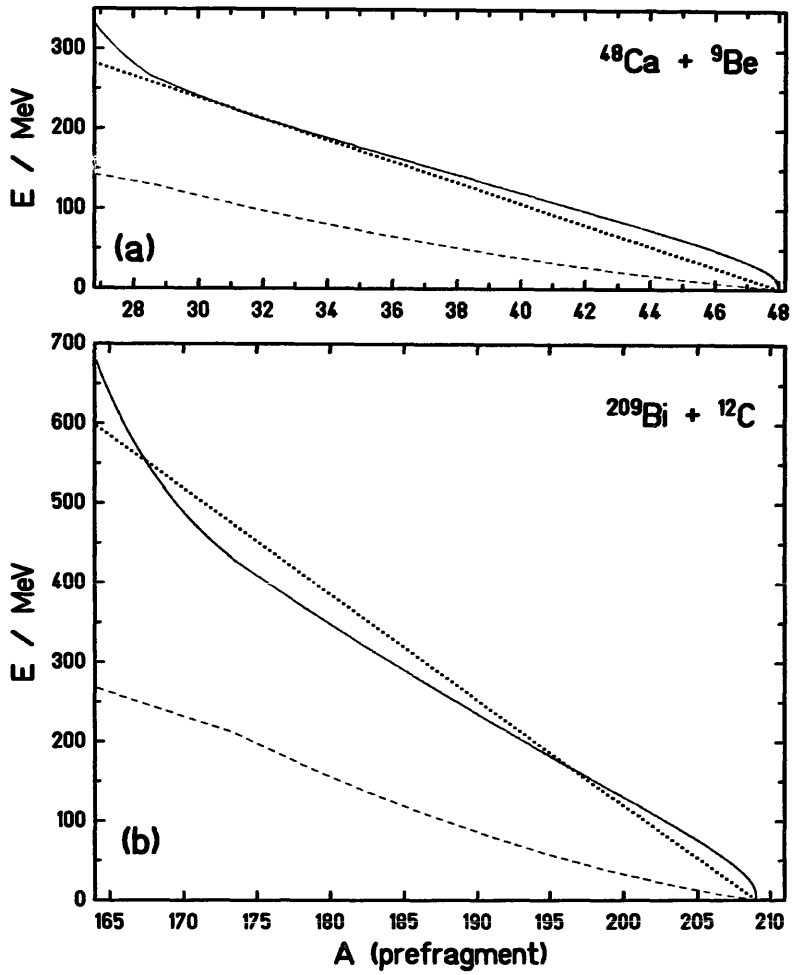

Fig. 1. Excitation energy after the abrasion process as a function of the prefragment mass for the systems ^{48}Ca+^{9}Be (a) and ^{209}Bi+^{12}C (b), calculated with three different models: Dashed line: geometrical abrasion model [2]) which relates the excitation energy to the surface excess. Full line: extended version of the abrasion model [28]) with friction included. Dotted line: diabatic model (this work) which relates the excitation energy to the single-particle vacancies.

distribution of the prefragments with more nucleons removed is given by the convolution of several of these linear distributions as is demonstrated in fig. 2.

The statistical hole-energy model shows a close correspondence to the model of Goldhaber [33]) which relates the width of the momentum distribution of the fragments to the statistical distribution of the Fermi momenta of the removed nucleons. In the same spirit, Abul-Magd *et al.* [34]) linked the average induced longitudinal momentum to the removal of bound nucleons in the abrasion process.

3.2. STATISTICAL APPROACH FOR THE ANGULAR MOMENTUM OF THE PREFRAGMENT

With a statistical approach, similar to that proposed by Goldhaber [33]) for the linear momentum of the fragmentation products, it is possible to estimate the angular momentum of the prefragment.

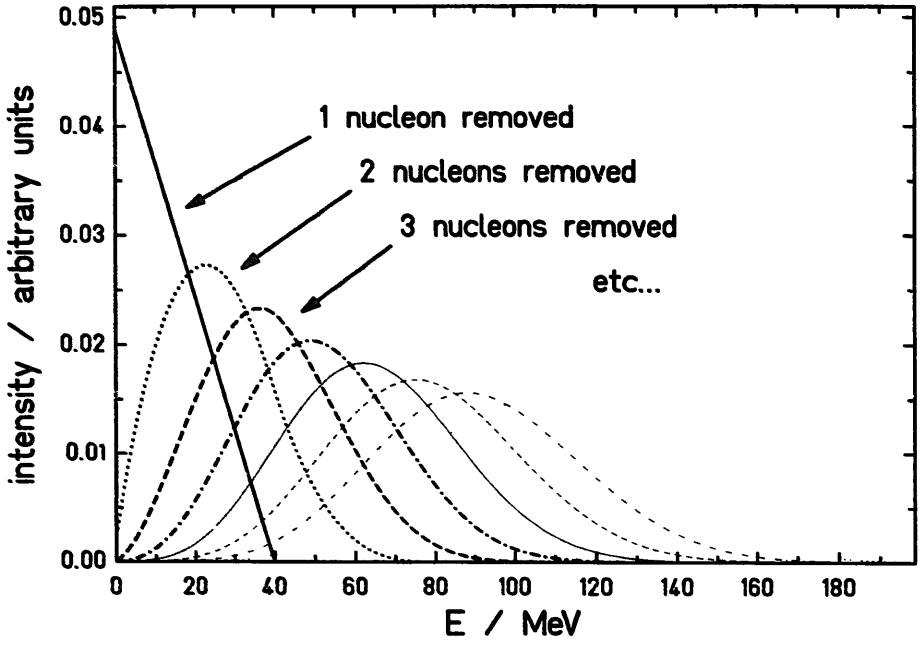

Fig. 2. Excitation-energy distributions as calculated with the diabatic model (this work) for different prefragments, after the abrasion of 1-8 nucleons from the projectile nucleus.

According to Goldhaber, the abrasion process causes a Gaussian momentum distribution which reflects the Fermi motion of the nucleons in the nucleus. In this model, the mean quadratic width of the momentum distribution is given by:

$$\langle P^2\rangle = \langle p^2\rangle \frac{A(A_p - A)}{A_p - 1}, \tag{3.6}$$

where A and A_p are the mass numbers of the fragment and the initial projectile, respectively, and $\langle p^2\rangle$ is the mean square value of the momenta of the nucleons which is equal to $\frac{3}{5}p_F^2$ with p_F being the Fermi momentum. The projection on a specific cartesian axis is given by replacing $\langle p^2\rangle$ by $\sigma_0^2 = \frac{1}{3}\langle p^2\rangle$. The experimental value for σ_0 is found to be constant as predicted but about 10% below the theoretical value. Nuclear-absorption effects were proposed to explain part of this discrepancy [35]). However, this discrepancy is not surprising because in relation (3.6) the total mass loss $A_p - A$ is attributed to the abrasion process. In a more realistic description, part of the mass loss should be attributed to the evaporation process which is expected to have less impact on the momentum width.

In a statistical model, the mean squared angular momentum of the prefragment is given in analogy to the above-mentioned description:

$$\langle J^2\rangle = \langle j^2\rangle \frac{A'(A_p - A')}{A_p - 1}, \tag{3.7}$$

where A' is the mass number of the prefragment and $\langle j^2\rangle$ is the quadratic mean value of the angular momentum of a nucleon in the nucleus. According to the shell model [36]), this value grows with the mass number of the nucleus from $1.3\hbar^2$ for ^{16}O,

$6.9\hbar^2$ for ^{88}Sr to $13.3\hbar^2$ for ^{208}Pb. We estimate the root-mean-square angular momentum for some specific cases: for a prefragment ^{46}Ca from a ^{48}Ca projectile $\sqrt{\langle J^2\rangle} = 2.9\hbar$ is expected, for a prefragment ^{200}Au from ^{208}Pb we get $\sqrt{\langle J^2\rangle} = 10.1\hbar$.

This approach shows that the angular momenta introduced by the abrasion process in peripheral collisions are of the order of $(3\text{–}10)\hbar$. This value is expected to be essentially preserved up to the end of the deexcitation process, because the centrifugal barrier favours the evaporation of particles with low angular momenta. There exists a direct experimental indication for the angular momentum, induced by the abrasion process. In combination with the deflection of the fragments by the mean field of the target spectators it has been exploited for producing polarized secondary beams [37,38]).

3.3. MODIFICATIONS TO THE EVAPORATION MODEL

The emission of a particle j in an evaporation process from the excited nucleus with neutron number N, proton number Z, angular momentum J, and excitation energy E is characterized by the emission width Γ_j which can be calculated by the statistical model. The emission probability of the particle j is determined by:

$$W_j(N, Z, E) = \frac{\Gamma_j(N, Z, E)}{\sum_k \Gamma_k(N, Z, E)}, \tag{3.8}$$

whereby the angular momentum is not considered explicitly. The ratio of the different emission widths for protons ($j = \mathrm{p}$), neutrons ($j = \mathrm{n}$), and α-particles ($j = \alpha$) can be approximated by the ratio of the level densities at the average excitation energies of the daughter nuclei

$$E_\mathrm{d} = E - S_j - B_{j\,\mathrm{eff}} - e'_j,$$

with the separation energy S_j, the effective Coulomb barrier $B_{j\,\mathrm{eff}}$ (which includes an average tunneling effect and is thus lower than the potential barrier), and the average kinetic energy $e'_j = 2t$ of the evaporated particle:

$$\frac{\Gamma_\mathrm{p}}{\Gamma_\mathrm{n}}(N, Z, E) = \frac{\Omega(N, Z-1, E - S_\mathrm{p} - B_{\mathrm{p\,eff}} - 2t)}{\Omega(N-1, Z, E - S_\mathrm{n} - 2t)}, \tag{3.9}$$

$$\frac{\Gamma_\alpha}{\Gamma_\mathrm{n}}(N, Z, E) = \frac{\Omega(N-2, Z-2, E - S_\alpha - B_{\alpha\,\mathrm{eff}} - 2t)}{2\Omega(N-1, Z, E - S_\mathrm{n} - 2t)}, \tag{3.10}$$

with the nuclear temperature $t = \sqrt{E_\mathrm{d}/\tilde{a}}$ and $\tilde{a}$ being the level-density parameter.

We will use these emission probabilities of neutrons, protons and alpha particles as the new statistical weights for calculating the mean values of α, e, τ_1 and τ_2 for one evaporation step of the model of Campi and Hüfner, which correspond to the change of the average mass, excitation energy, neutron excess, and quadratic width in neutron excess of the system, respectively. As a consequence of this modification,

we are obliged to calculate the values of α, e, τ_1 and τ_2 for each evaporation step i separately:

$$\alpha_i = \langle \Delta A \rangle_i = W_{ni} \cdot 1 + W_{pi} \cdot 1 + W_{\alpha i} \cdot 4 , \tag{3.11}$$

$$e_i = \langle \Delta E \rangle_i = W_{ni} \cdot S_n(A_{i-1}, I_{i-1}) + W_{pi} \cdot [S_p(A_{i-1}, I_{i-1}) + B_{p\,\mathrm{eff}}(A_{i-1}, I_{i-1})] + W_{\alpha i} \cdot [S_\alpha(A_{i-1}, I_{i-1}) + B_{\alpha\,\mathrm{eff}}(A_{i-1}, I_{i-1})] + 2\sqrt{E_i/\tilde{a}} , \tag{3.12}$$

$$\tau_{1i} = \langle \Delta I \rangle_i = W_{ni} \cdot (+1) + W_{pi} \cdot (-1) + W_{\alpha i} \cdot 0 , \tag{3.13}$$

$$\tau_{2i} = \langle (\Delta I - \langle \Delta I \rangle_i)^2 \rangle_i = W_{ni} \cdot (1 - \langle \Delta I \rangle_i)^2 + W_{pi} \cdot (-1 - \langle \Delta I \rangle_i)^2 + W_{\alpha i} \cdot (0 - \langle \Delta I \rangle_i)^2 , \tag{3.14}$$

where $W_{ji} = W_j(A_{i-1}, I_{i-1}, E_{i-1})$ with $j = \mathrm{n}, \mathrm{p}, \alpha$, and the system after the ith step is defined by (A_i, I_i, E_i) such that:

$$A_i = A_{i-1} - \alpha_i , \tag{3.15}$$

$$I_i = I_{i-1} - \tau_{1i} , \tag{3.16}$$

$$E_i = E_{i-1} - e_i . \tag{3.17}$$

These average values depend on the properties of the mother nucleus as well as on the daughter nucleus in every evaporation step, that means on the mass number, neutron number, and excitation energy of the nucleus. Table 2 shows these average values for some nuclei at different excitation energies in comparison with the constant mean values of the original evaporation model. In particular for the rather neutron-rich nucleus ^{48}Ca, the new approach gives drastically different numbers for the mean change of neutron excess. This number is decisive for the direction on the chart of nuclides which is taken by the evaporation process.

TABLE 2

Properties of the average particle emitted in the first step ($i = 1$) of the evaporation process as calculated with the modified evaporation model in comparison to the original model as proposed by Campi and Hüfner [18]). See text for explanation

Nucleus (excitation energy)	Mean values of the modified model ($i = 1$)				Constant mean values of the Campi and Hüfner model			
	α_i	e_i	τ_{1i}	τ_{2i}	α	e	τ_1	τ_2
^{48}Ca (200 MeV)	1.05	16.41	0.69	0.51	1.6	20	0	0.8
^{48}Ca (150 MeV)	1.05	15.26	0.76	0.42				
^{48}Ca (100 MeV)	1.04	13.90	0.84	0.28				
^{48}Ca (50 MeV)	1.02	12.07	0.95	0.09				
^{42}Ca (50 MeV)	1.16	10.80	−0.10	0.94				
^{40}Ca (50 MeV)	1.14	8.03	−0.65	0.53				

In the modified evaporation model the mass number A of the final fragment is related to the mass number A' of the prefragment by:

$$A = A' - \sum_{i=1}^{i_{max}} \alpha_i , \tag{3.18}$$

with i_{max} defined by the relation:

$$E' - E_t < \sum_{i=1}^{i_{max}} e_i \leq E' , \tag{3.19}$$

whereby E_t is the lowest threshold energy for particle emission from the final nucleus. The gaussian, resulting from the diffusion process, which is also named memory factor of the expression (2.5) in the model of Campi and Hüfner is replaced by:

$$\exp \frac{-[I - (I' - \sum_{i=1}^{i_{max}} \tau_{1i})]^2}{2 \sum_{i=1}^{i_{max}} \tau_{2i}} , \tag{3.20}$$

with I and I' being the neutron excess of the final fragment and of the prefragment, respectively. The other parts of eq. (2.5) remain unchanged.

We compared the modified evaporation model as well as the original model of Campi and Hüfner to the statistical evaporation code CODEX [39]). We considered two nuclei, ^{40}Ca and ^{48}Ca at three different excitation energies between 50 and 200 MeV. Fig. 3 shows the calculated final distributions of the fragments after evaporation. The direction of the evaporation process, calculated with the modified model, coincides well with the result of the statistical evaporation code. The results of these two models converge towards a common corridor, whereas the original evaporation model of Campi and Hüfner predicts two distinctly different evaporation paths, starting from the excited nuclei ^{40}Ca and ^{48}Ca. We think that the original evaporation model of Campi and Hüfner, intended to make the evaporation process more transparent, will become essentially more realistic by the modifications proposed above.

3.4. MICROSCOPIC STRUCTURES IN THE STATE DENSITY

The experimental observation shows that there is a strict correspondence between the microscopic corrections of the nuclear binding energies in the ground state and those of the level densities. We want to investigate this relation in detail and discuss its significance for the fragmentation cross sections.

Besides the microscopic contribution to the ground-state binding energy, defined as the difference of the experimental mass [40]) and the mass of the liquid-drop model [41,42]), the relative experimental energies of some nth state are traced in figs. 4a, 5a and 6a, whereby n is limited by the experimental knowledge. The states were counted with the weight of their degeneracy. Fig. 4a shows the microscopic corrections, caused by pairing and shell effects, as observed in light nuclei. Fig. 5a illustrates the shell corrections for heavier nuclei whereas fig. 6a demonstrates the pairing

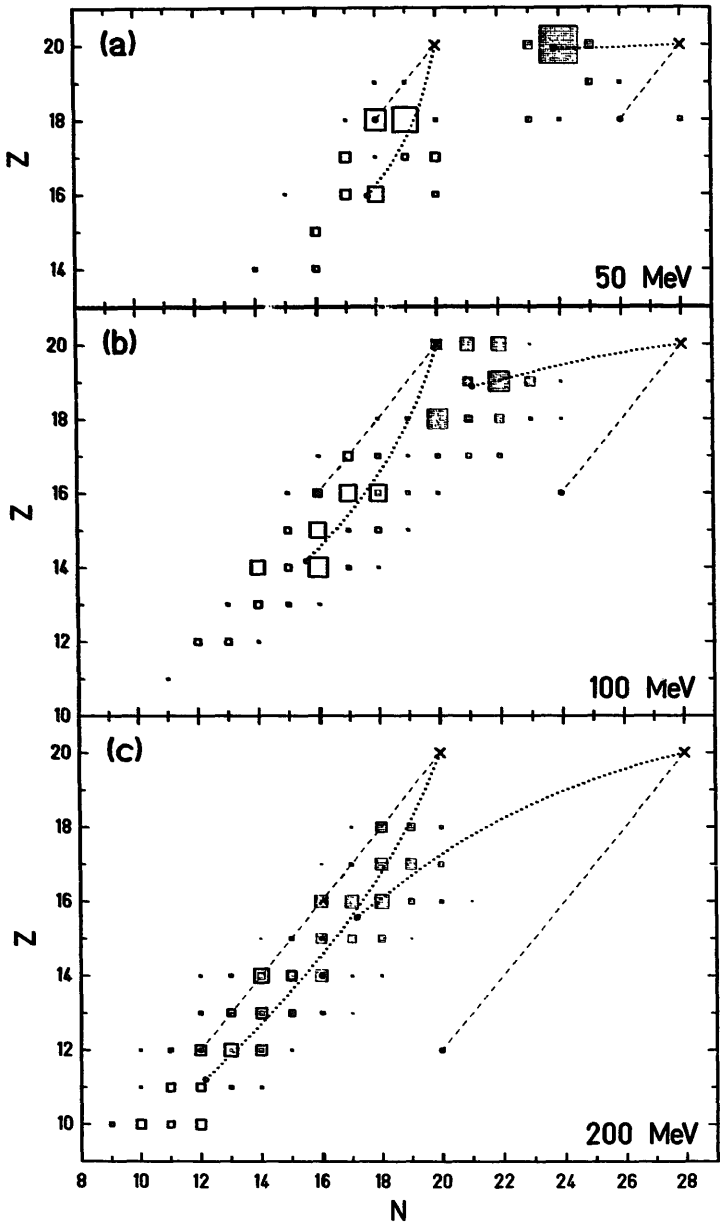

Fig. 3. Results of evaporation calculations on a chart of nuclides. The compound nuclei ^{40}Ca and ^{48}Ca, marked by crosses, are considered at excitation energies of 50 MeV (a), 100 MeV (b) and 200 MeV (c). Open and hatched squares: evaporation-residues emerging from the two compound nuclei as calculated with the Monte Carlo code CODEX [39]). Dashed lines: mean evaporation paths as calculated with the macroscopic evaporation model of Campi and Hüfner [18]). Dotted lines: mean evaporation paths as calculated with the modified macroscopic evaporation model (this work) which includes the statistical weights of the residual states in each evaporation step.

corrections for heavier nuclei. As an example for light nuclei we chose a series with $A/Z = 2$ from C to Ar. As representatives for heavier nuclei we chose isotopes of the elements Kr and Mo across the 50-neutron shell.

According to the figures, we state that the structure of the energies of the nth state compensates more or less for the microscopic structure of the nuclear masses. Experimentally, the microscopic structure of the nuclei in their ground state is

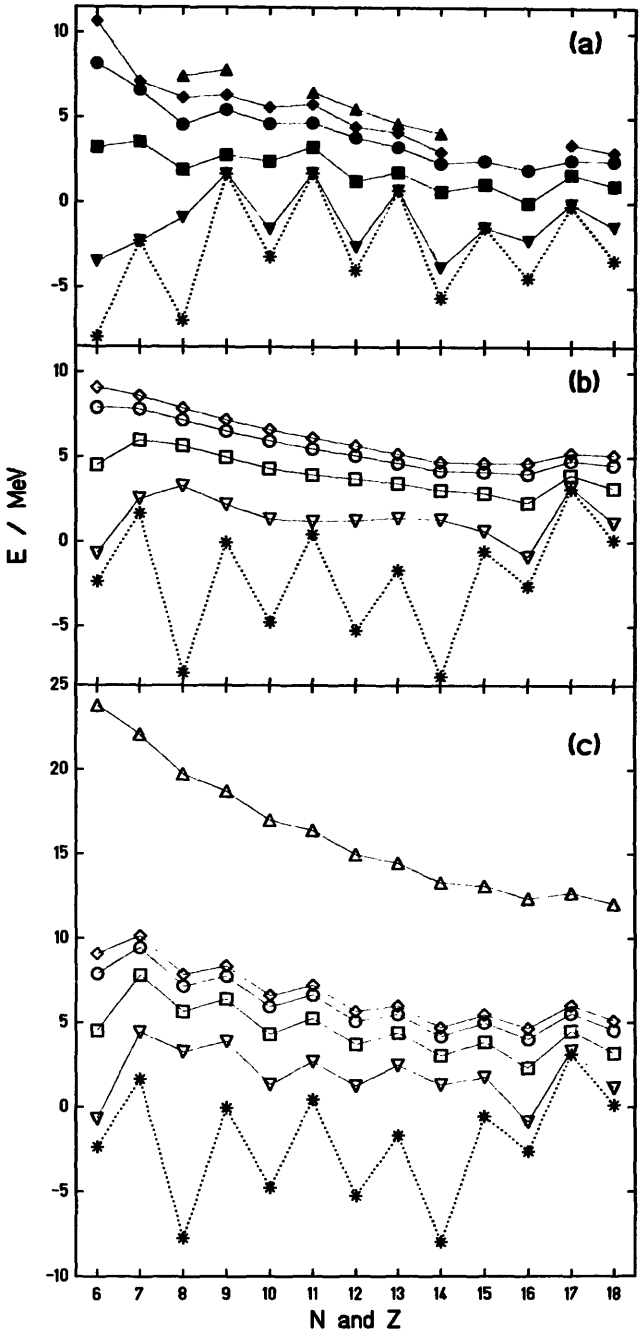

Fig. 4. Microscopic corrections of light even-mass nuclei with $A/Z = 2$ from carbon to argon in the binding energies and in the level densities. (a) Experimental values: the asterisks give the experimental microscopic corrections to the binding energies as given by the differences of the experimental masses [40]) and those of the liquid-drop model [41,42]). The other symbols give the sum of the experimental microscopic corrections to the binding energies and the measured excitation energies of the 2nd, the 21st, the 60th, the 93rd and the 151st level according to refs. [43-47]). (b) Calculated values: the asterisks give the microscopic corrections to the binding energies as given by Myers and Swiatecki [41,42]). The other symbols give the sum of these microscopic corrections and the calculated excitation energies of the 2nd, 21st, 60th and 93rd level according to the level-density model of Ignatyuk *et al.* [67,68]). (c) Calculated values like (b), however the level density model was modified by the inclusion of a pairing fine-structure term (this work) (see text). In addition to (b) the points corresponding to the 3×10^4th level are included.

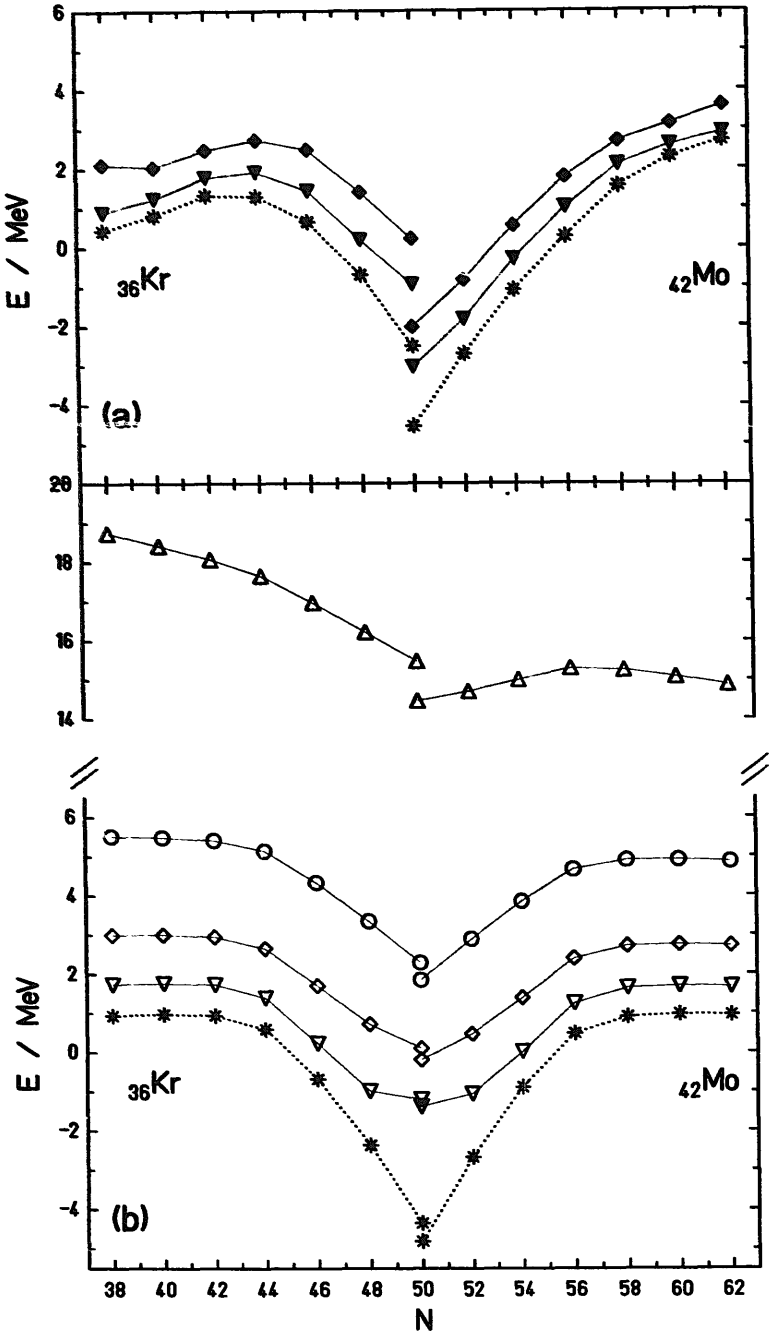

Fig. 5. Microscopic corrections of even-even isotopes of Kr and Mo near the $N = 50$ shell in the binding energies and in the level densities. (a) Experimental values: the asterisks give the experimental microscopic corrections to the binding energies as given by the differences of the experimental masses [40]) and those of the liquid-drop model [41,42]). The other symbols give the sum of these microscopic corrections and the measured excitation energies of the 2nd and the 21st level according to refs. [48-61]). (b) Calculated values: the asterisks give the microscopic corrections to the binding energies as given by Myers and Swiatecki [41,42]). The other symbols give the sum of these microscopic corrections and the calculated excitation energies of the 2nd, 21st, 400th and 10^{19}th level according to the level-density model of Ignatyuk *et al.* [67,68]).

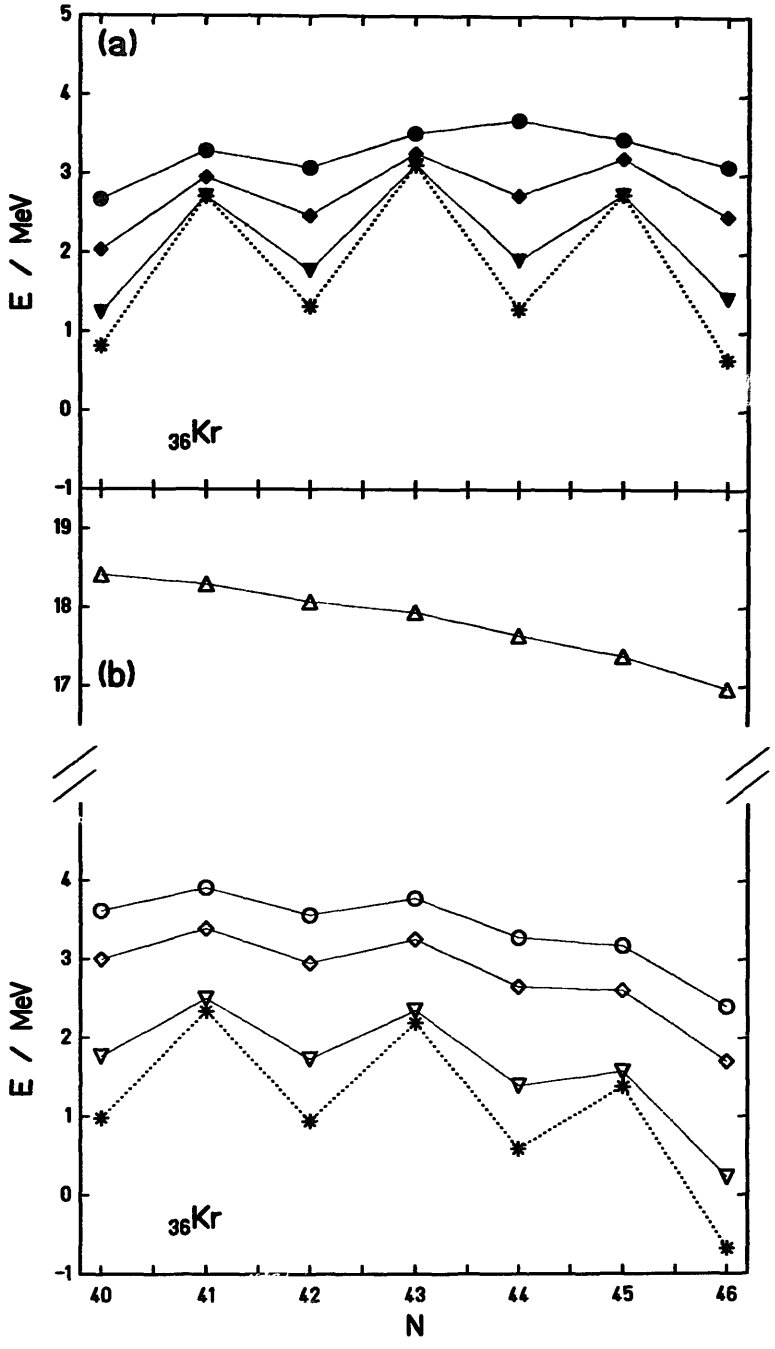

Fig. 6. Microscopic corrections of Kr isotopes in the binding energies and in the level densities. (a) Experimental values: the asterisks give the experimental microscopic corrections to the binding energies as given by the differences of the experimental masses [40]) and those of the liquid-drop model [41,42]). The other symbols give the sum of these microscopic corrections and the measured excitation energies of the 2nd, the 21st and the 44th level according to refs. [51,54,57,59,62-64]). (b) Calculated values: the asterisks give the microscopic corrections to the binding energies as given by Myers and Swiatecki [41,42]). The other symbols give the sum of these microscopic corrections and the calculated excitation energies of the 2nd, 21st, 44th and 10^9th level according to the level-density model of Ignatyuk *et al.* [67,68]), including a pairing fine-structure term (this work) (see text).

washed out with increasing energy. The microscopic structure of the light nuclei is already mostly destroyed from the 21st state on. However, some odd-even structure persists even beyond this state, that means for higher excitation energies. For heavier nuclei the odd-even structure is mostly destroyed from the 44th state on which corresponds to rather low excitation energies. There are not enough experimental data available in order to decide whether an odd-even fine structure persists at higher energies like that observed for lighter nuclei. In contrast to the pairing structure, the 50-neutron shell effect in the level density is much less affected by an increasing excitation energy.

There exist microscopic calculations of the nuclear level density (e.g. ref. [65])) which include the effects of shell and pairing correlations. The resulting washing-out of shell effects [65,66]) was parametrized by Ignatyuk *et al.* [67]) by an exponential function. For the differences between odd-odd, odd-mass and even-even nuclei, Ignatyuk *et al.* [68]) proposes a backshift of $-\Delta_0$ for odd-mass and $-2\Delta_0$ for even-even nuclei, where $\Delta_0 \approx 12\ \mathrm{MeV}/\sqrt{A}$ is the pairing gap. This model destroys all pairing structure already for the first excited state of the nucleus. In fig. 4b the model predictions including shell effects [67]) and pairing [68]) in the level density are shown. Obviously this model fails to predict the remaining pairing structure of these light nuclei at high energies.

The microscopic models, based on the BCS theory [69,70]), predict a sharp phase transition between a superfluid domain below and a normal domain above the critical temperature which itself depends on the angular momentum. However, more realistic considerations of Ignatyuk *et al.* [71]) and Egido *et al.* [72]) showed that the phase transition of a finite nuclear system is not sharp and that pairing correlations persist partly even at very high energies. To our knowledge there exists no model calculation of the nuclear level density with the degree of sophistication needed to reproduce the subtle behaviour of the odd-even structure as shown in fig. 4a.

In the evaporation model of Campi and Hüfner, the fragmentation cross sections are strongly related to the phase space of the observable final nuclei below the particle threshold. In order to investigate structural influences on the fragmentation, we applied the following microscopic corrections: To reproduce the pairing fine structure observed at higher energies, we introduced a new effective excitation energy

$$E^* = \begin{cases} E & \text{for even-even nuclei} \\ E + \Delta_0 - \delta'' & \text{for odd-mass nuclei} \\ E + 2\Delta_0 - 2\delta'' & \text{for odd-odd nuclei} \end{cases}$$

with $\delta'' = 28\ \mathrm{MeV}\, h'(E)/A^{1.1}$ and $h'(E) = \exp(-E/E_c)$, according to a suggestion of Ignatyuk [73]).

The complete description of the state density reads as follows:

$$\Omega(E) = \frac{\sqrt{\pi}\exp(S)}{12E^{5/4}\tilde{a}^{1/4}}, \tag{3.21}$$

where S is the entropy, and

$$\tilde{a} \simeq \frac{A}{14.61}(1+3.114A^{-1/3}+5.626A^{-2/3})\ \mathrm{MeV}^{-1} \tag{3.22}$$

is the structureless level-density parameter according to ref. [74]). At lower energies, we use the expressions for the non-interacting Fermi gas given by Grossjean and Feldmeier [75]) which removes the singularity at $E=0$ of the expression (3.21). The

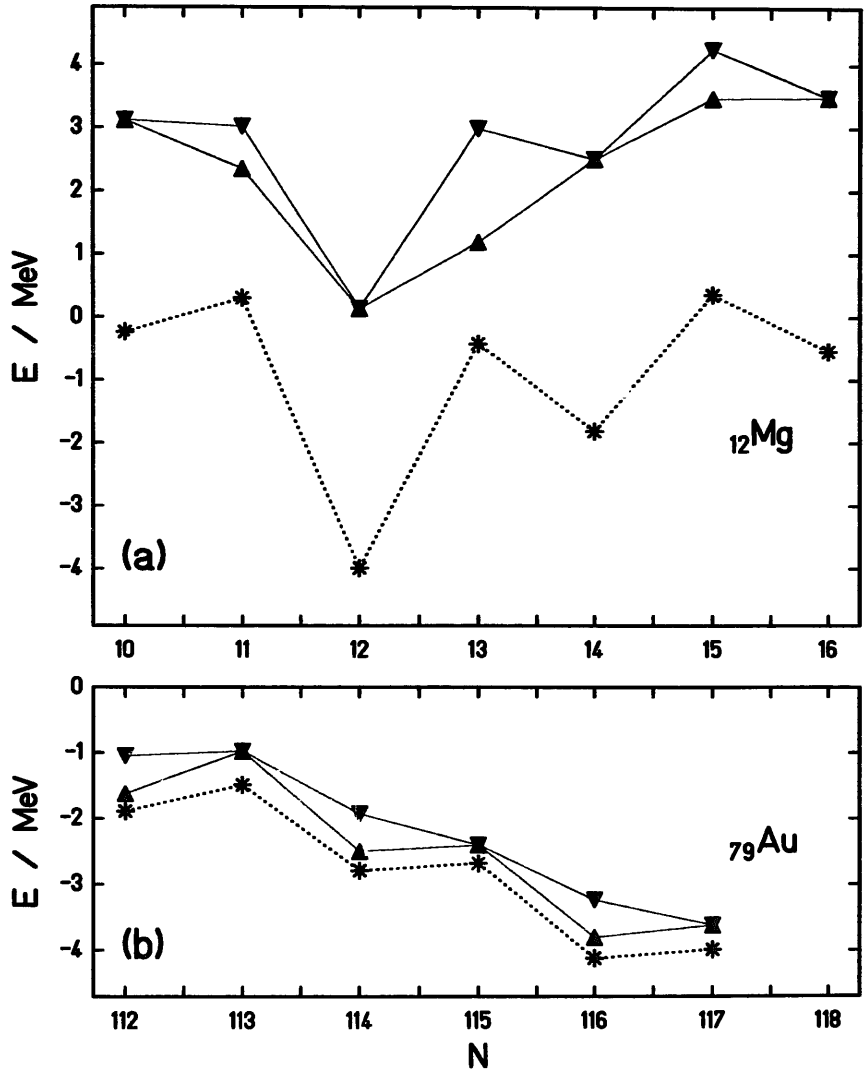

Fig. 7. (a) Microscopic corrections of Mg isotopes in the binding energies at specific angular momenta. The asterisks give the experimental microscopic corrections to the binding energies as given by the differences of the experimental masses [40]) and those of the liquid-drop model [41,42]). The other symbols give the sum of these microscopic corrections and the measured excitation energies [43]) of the lowest $J=4$ states for even isotopes (⧗) as well as for the $J=\frac{7}{2}$ states (▲) and $J=\frac{9}{2}$ (▼) states for odd isotopes. (b) Microscopic corrections of Au isotopes in the binding energies at specific angular momenta. The asterisks give the experimental microscopic corrections to the binding energies as given by the differences of the experimental masses [40]) and those of the liquid-drop model [41,42]). The other symbols give the sum of these microscopic corrections and the measured excitation energies [77-82]) of the lowest $J=6$ states for odd isotopes (⧗) as well as for the $J=\frac{11}{2}$ states (▲) and $J=\frac{13}{2}$ (▼) states for even isotopes.

microscopic corrections are introduced in the entropy by

$$S = 2\sqrt{\tilde{a}(E^* + U' f(E^*) - 2\Delta_0 h(E^*))}\,, \tag{3.23}$$

where E^* is the effective energy, U' is the nuclear ground-state shell correction,

$$f(E^*) = 1 - \exp(-\gamma E^*) \tag{3.24}$$

describes the washing-out of shell effects [67]) with the parameter γ determined by [30])

$$\frac{1}{\gamma} \simeq 0.4 \frac{A^{4/3}}{\tilde{a}}\,, \tag{3.25}$$

$$h(E^*) = \begin{cases} E^*/2\Delta_0 + (1 - E_c/2\Delta_0)E^{*2}/E_c^2 & \text{for } E^* < E_c \\ 1 & \text{for } E^* \geqslant E_c \end{cases}$$

parametrizes the superfluid phase transition [68]) at $E_c = 10$ MeV [ref. [76])]. In figs. 4c, 5b and 6b the predictions of this model are included. They reproduce the structure of the data in a satisfactory way.

Another point of interest is the variation of the microscopic odd–even structure as a function of the angular momentum of the nucleus. This is even more important as the evaporation chain after the abrasion step takes place at somewhat higher angular momenta (see sect. 3.2). Fig. 7 shows the experimental microscopic structure of the yrast line for gold isotopes at the angular momenta $6\hbar$, $\frac{11}{2}\hbar$ and $6\hbar$, $\frac{13}{2}\hbar$ and for the magnesium isotopes at the angular momenta $4\hbar$, $\frac{7}{2}\hbar$ and $4\hbar$, $\frac{9}{2}\hbar$. On the average, the odd–even structure disappears partly with increasing angular momentum.

4. Comparison of the fragmentation model to experimental data

In this chapter the modified fragmentation model as developed in the preceding chapter will be compared to the body of experimental data available as well as to some previously used model descriptions. However, the angular-momentum distribution is not included in the actual version of the modified model. The predicted width of the excitation-energy distribution of the prefragments destroys the one-to-one correspondence between prefragment and fragment mass of the original model. As a consequence, a summation over all prefragments which end up at a certain fragment after evaporation is performed. The full expressions of the modified model are summarized in ref. [83]).

In the first part we will stress the importance of a realistic evaporation model. Secondly we will test different descriptions of the excitation energy and of the charge distribution of the prefragments. In the third part we will discuss the role of microscopic effects on the fragmentation cross sections, and we will investigate the odd–even structure observed in the cross sections of light even-mass fragments. All calculations in this chapter are performed without any adjusted parameter.

4.1. INFLUENCE OF THE EVAPORATION PROCESS ON THE ISOTOPIC DISTRIBUTION

The first experimental data to which the model calculations will be compared are the production cross sections of neutron-rich gold isotopes, obtained by the fragmentation of a ^{209}Bi target with a ^{12}C beam of 400 MeV/u [ref. [84])]. The fragmentation of ^{209}Bi is a very interesting test case for our model. This nucleus is very far from the equilibrium-residue corridor. The fission barrier is still high enough that it is not too important that our model does not include fission. The isotopic distribution of gold which differs in proton number only by four units from that of bismuth is an excellent test for the influence of the memory factor on the fragment distribution.

The experimental data are shown in fig. 8. They are compared to cross sections calculated with the macroscopic evaporation model of Campi and Hüfner with different approaches for the excitation energy and the charge distribution of the prefragments on the one hand, and to predictions of the modified macroscopic evaporation model on the other hand. The disagreement between the evaporation model of Campi and Hüfner and these experimental data is caused by the mean change of neutron excess per evaporated particle assumed to be zero in this model. The modified evaporation model with statistical weights introduced reproduces well the experimental data if a rather high excitation energy is deposited in the prefragment and if a broad charge distribution is chosen. This is the case if the excitation energy is calculated by the extended abrasion model or by the proposed statistical hole-energy model. The appropriate charge distribution of the prefragment is that of the hypergeometrical model. A narrow charge distribution like that deduced from the GDR cannot reproduce the slope of the experimental isotopic cross-section distribution.

In a more general presentation, fig. 9 shows the yields of the final nuclei on a chart of nuclides as calculated with the macroscopic model of Campi and Hüfner and with the modified macroscopic evaporation model. According to the latter, the evaporation of neutrons is very pronounced and the distribution joins quickly the equilibrium-residue corridor. Fig. 10 illustrates the influence of the different factors in the modified macroscopic evaporation model for two isotopic distributions, namely the memory factor and the state-density factor.

In the following we will only present calculations with the modified macroscopic evaporation model.

4.2. THE INFLUENCE OF THE EXCITATION ENERGY AND THE CHARGE DISTRIBUTION OF THE PREFRAGMENTS ON THE CROSS SECTIONS

In figs. 11–15, the experimental isotopic cross sections of five elements, Cl, S, Al, Mg and O, are shown as produced in different projectile-fragmentation reactions. The first one corresponds to a ^{40}Ar beam at 600 MeV/u [ref. [85])] or at 213 MeV/u [ref. [86])] on a ^{12}C target, the second one to a ^{48}Ca beam at 212 MeV/u on a ^{9}Be target [87]). The specific interest in these data relies on the different neutron-to-proton

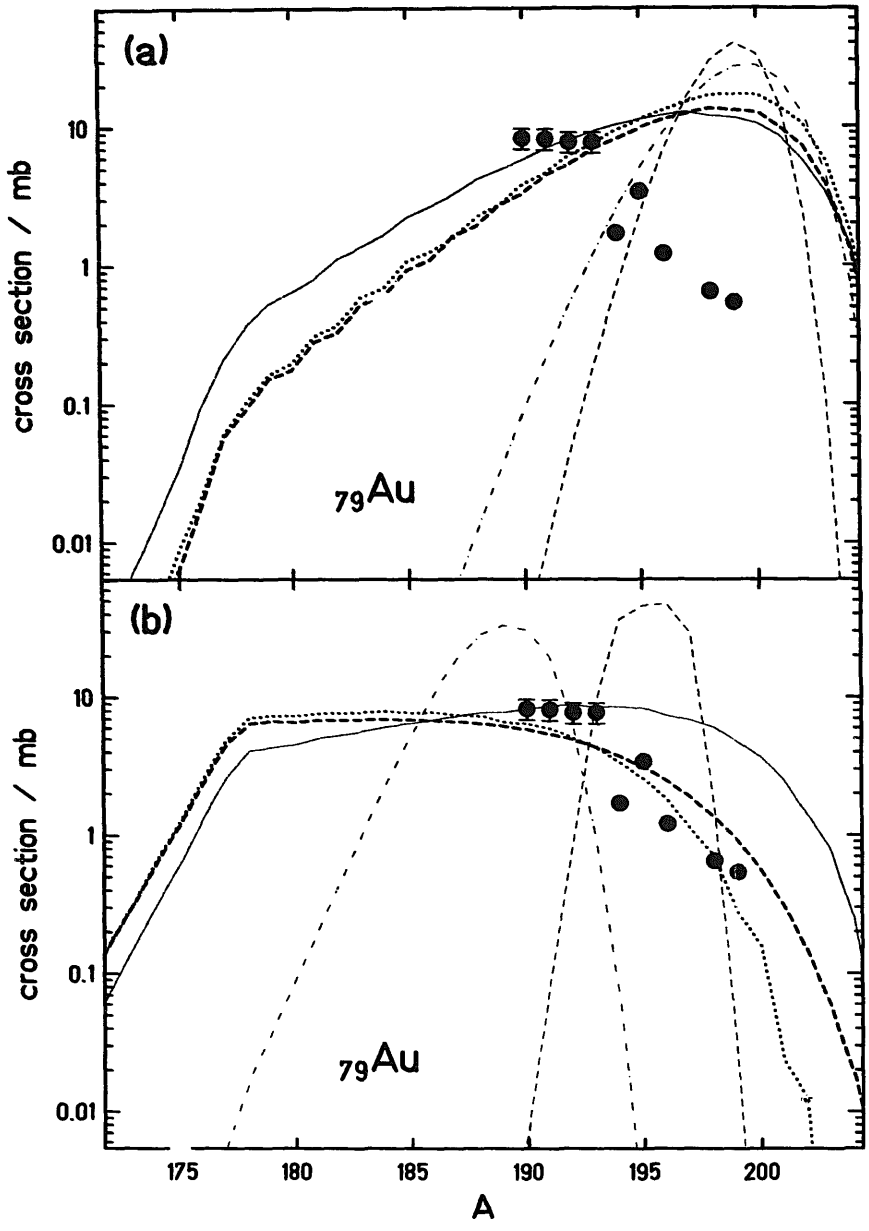

Fig. 8. Cross sections of Au isotopes produced in the fragmentation of ^{209}Bi target by ^{12}C (400 MeV/u). The data points are taken from ref. [84]). (a) Calculations with the original macroscopic evaporation model of Campi and Hüfner [18]). (b) Calculations with the modified macroscopic evaporation model including the statistical weights of the residual states in each evaporation step (this work). In both cases, different options for the charge distribution and the excitation energy of the prefragments have been used: Full lines: hypergeometrical model and surface energy [2]). Thin dashed lines: GDR model [21]) and surface energy [2]). Dotted lines: hypergeometrical model and surface energy plus friction [28]). Dash-dotted lines: GDR model [21]) and surface energy plus friction [28]). Thick dashed lines: hypergeometrical model and single-particle vacancy model (this work).

ratios of the two different projectiles. The experimental data show that the isotopic distribution of S produced by the ^{48}Ca beam preserves a neutron-rich composition, whereas the difference between the isotopic distributions produced in the two different reactions disappears progressively for the lighter elements.

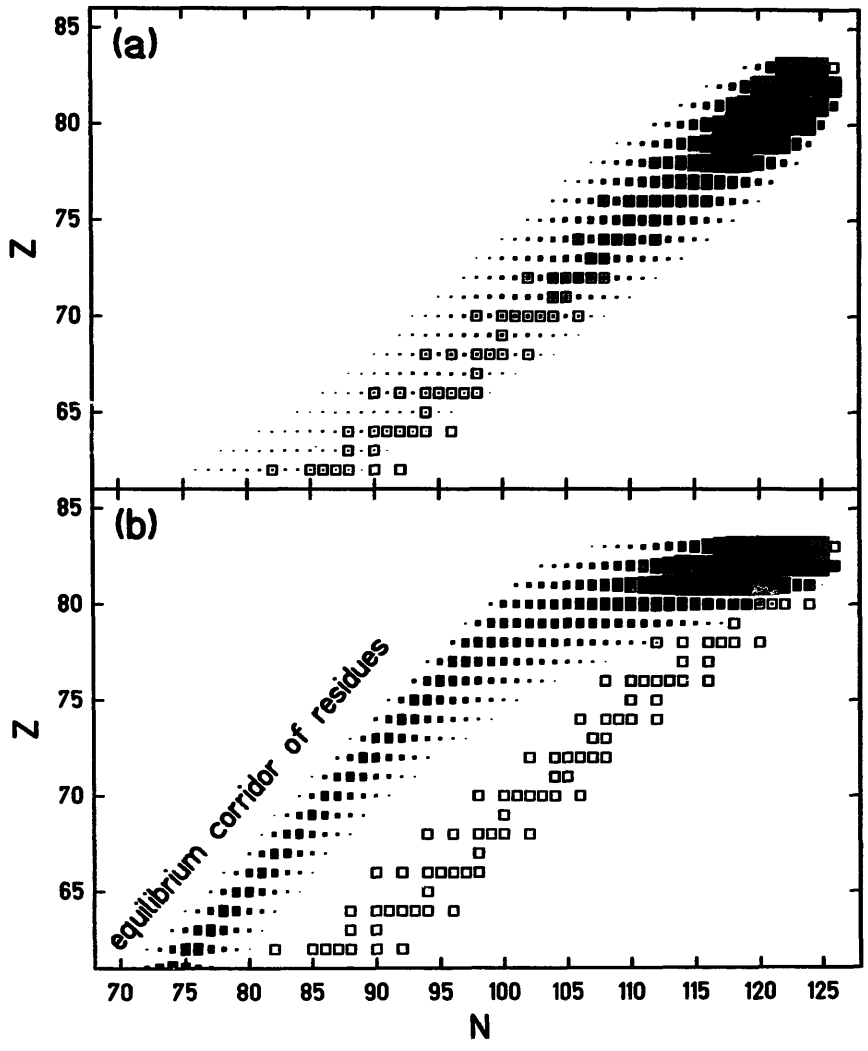

Fig. 9. Fragmentation products of ^{209}Bi on ^{12}C. The surface of the full squares corresponds to the production cross section. The smallest cross section shown is equal to 2 mb. The open squares indicate the premordial nuclei. (a) Calculation with the original macroscopic evaporation model of Campi and Hüfner [18]). (b) Calculation with the modified macroscopic evaporation model including the statistical weights of the residual states in each evaporation step (this work). In both cases, the hypergeometrical model and the single-particle vacancy model (this work) have been used for the charge distribution and the excitation energy of the prefragments, respectively. The results of the calculations do not depend on the projectile energy.

In addition to the experimental data, the results of different model calculations are shown. For these light fragments the best agreement is achieved with a rather low prefragment excitation energy as calculated from the surface-energy excess only or with the proposed statistical hole-energy model. However, there remain some systematic disagreements which we cannot explain: The observed cross sections of the neutron-rich Cl fragments produced by the ^{48}Ca beam are appreciably higher than the values calculated with any model, and the observed isotopic distribution of the elements O is narrower than predicted. The first discrepancy could only be removed by lowering the excitation energy even below the value estimated by the surface excess while the second one is only slightly decreased by assuming a closer

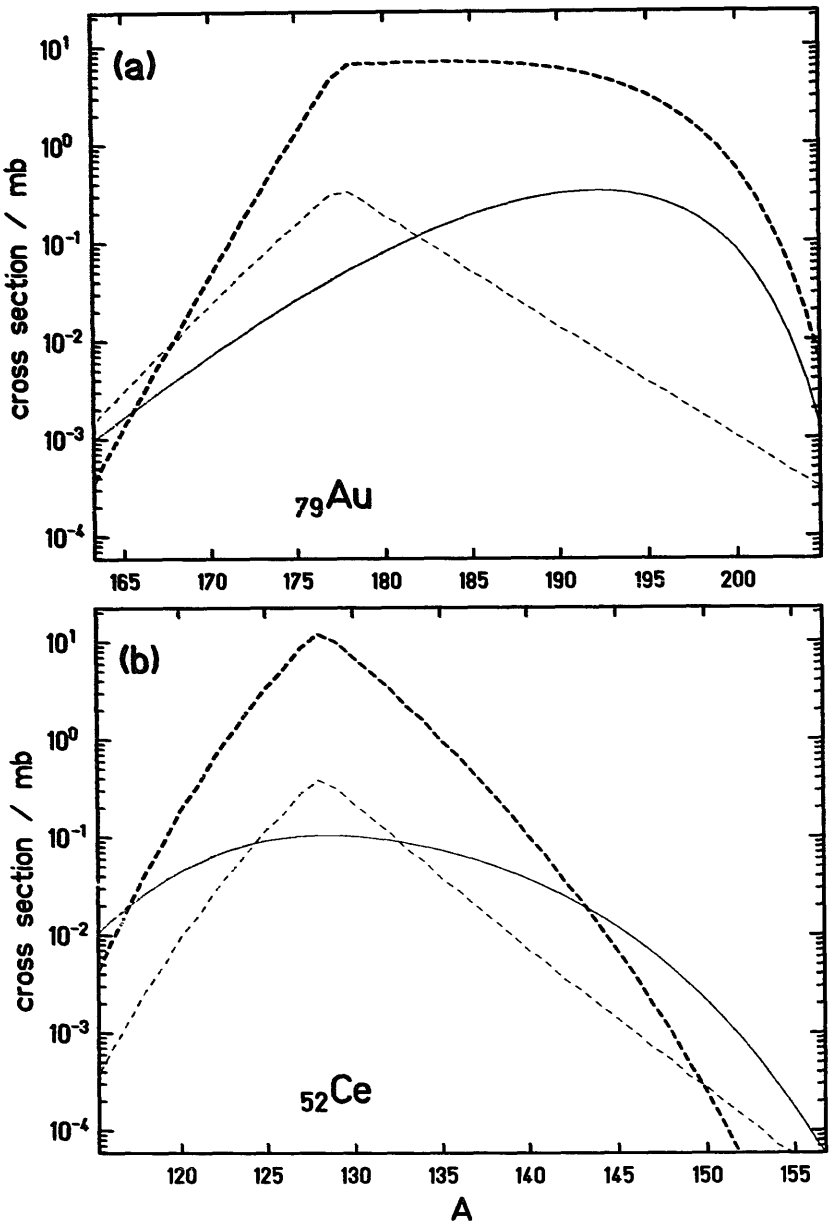

Fig. 10. Calculated cross sections of Au (a) and Ce (b) isotopes as calculated for the fragmentation of ^{209}Bi on ^{12}C (thick dashed lines). In addition, the memory term (full lines) and the equilibrium term (thin dashed lines) are given on an arbitrary scale as calculated with the modified macroscopic evaporation model (this work).

correlation between neutrons and protons during the abrasion. Another explanation could be a deficiency of the model which was used to calculate the ground-state masses of these nuclei.

In the comparison of the fragmentation of the heavier (^{209}Bi) and the lighter (^{40}Ar, ^{48}Ca) nuclei there is an interesting observation: The surface energy is appropriate to predict the isotopic distributions of the lighter systems (especially in figs. 11 and 12) while the one of the heavier system (fig. 8) is only reproduced by including frictional energy. However, the proposed statistical hole-energy model is able to

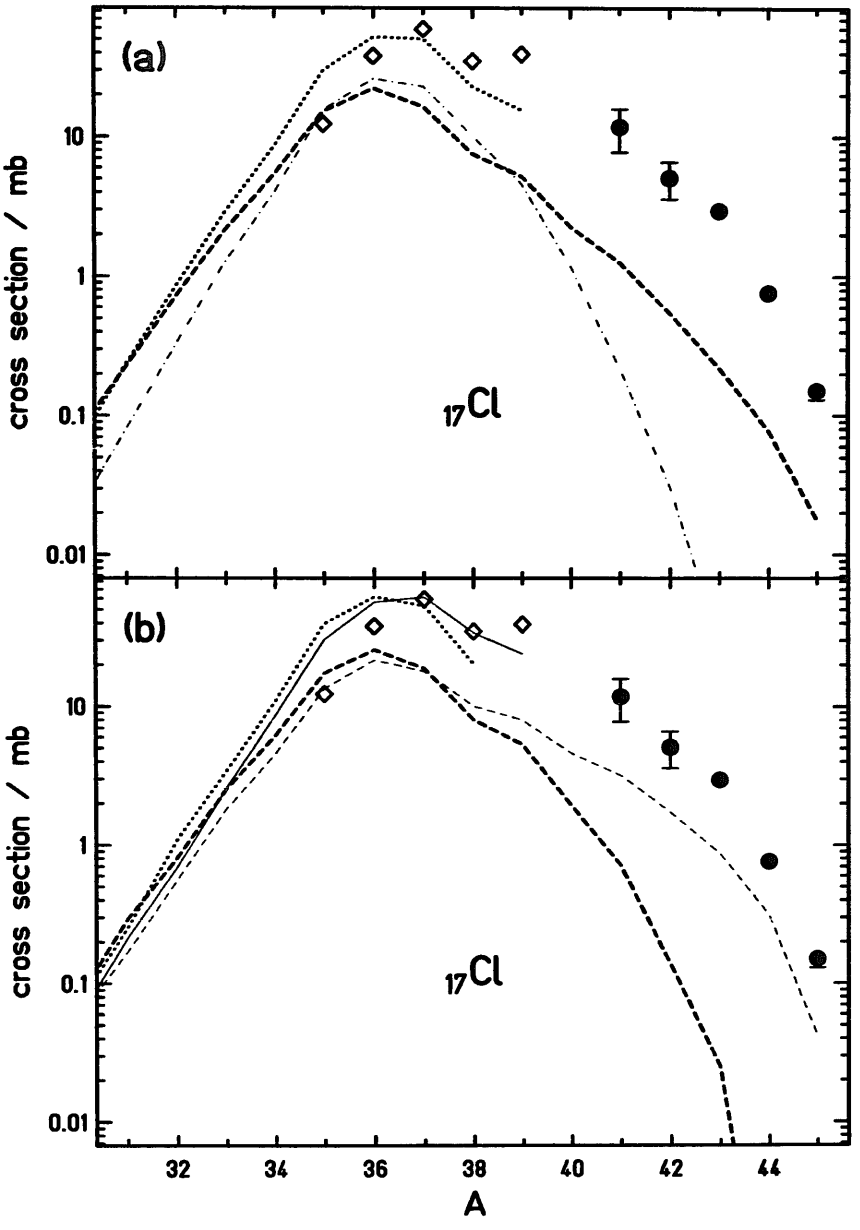

Fig. 11. Cross sections for the production of Cl isotopes in different projectile-fragmentation reactions. Open rhombs: experimental data of the reaction $^{40}Ar+^{12}C$ at 600 MeV/u [ref. [85])]. Full points: experimental data of the reaction $^{48}Ca+^{9}Be$ at 212 MeV/u [ref. [87])]. The curves are the results of model calculations for the two systems by use of the modified macroscopic evaporation model (this work). (a) The excitation energy of the prefragments is given by the diabatic single-particle vacancy model (this work). Different options for the charge distribution are used: Dotted line ($^{40}Ar+^{12}C$) and thick dashed line ($^{48}Ca+^{9}Be$): hypergeometrical model. Dash-dotted line ($^{48}Ca+^{9}Be$): GDR model [21]). (b) The charge distribution of the prefragments is given by the hypergeometrical model. Different options for the excitation energy of the prefragments are used: Full line ($^{40}Ar+^{12}C$) and thin dashed line ($^{48}Ca+^{9}Be$): surface energy [2]). Dotted line ($^{40}Ar+^{12}C$) and thick dashed line ($^{48}Ca+^{9}Be$): surface energy plus friction [28]).

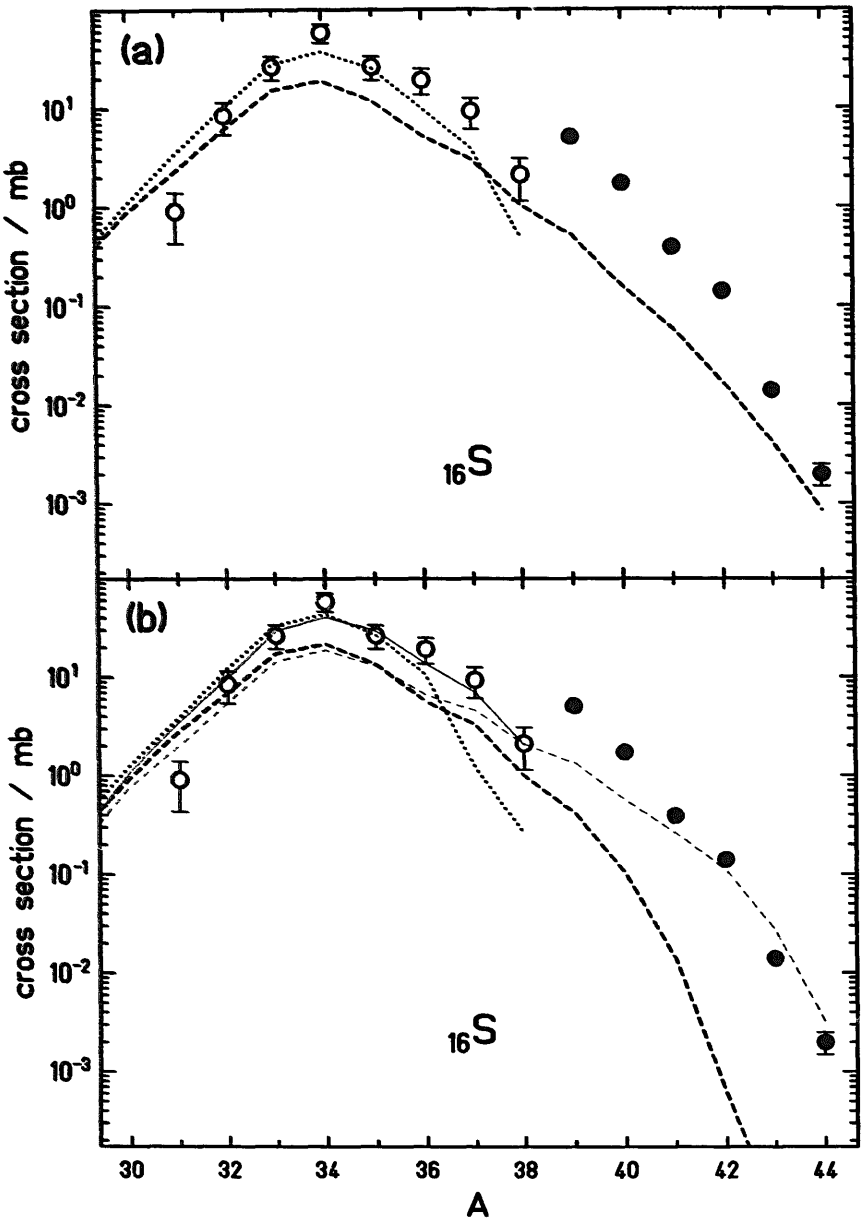

Fig. 12. Cross sections for the production of S isotopes in different projectile-fragmentation reactions. Open points: experimental data of the reaction $^{40}Ar+^{12}C$ at 213 MeV/u [ref. [86])]. Full points: experimental data of the reaction $^{48}Ca+^{9}Be$ at 212 MeV/u [ref. [87])]. The curves correspond to calculations as explained in fig. 11.

reproduce the main features of the measured isotopic distributions of both cases simultaneously. This is another argument in favour of the new model in contrast to the surface-energy model. Moreover, this means that the contribution of additional frictional effects to the excitation energy of the prefragments is rather low. Fig. 16 demonstrates the degree of agreement between experimental data and the predictions of the proposed model for some other fragmentation reactions. In addition, this investigation strongly favours a rather broad charge distribution of the prefragments as predicted by the hypergeometrical model.

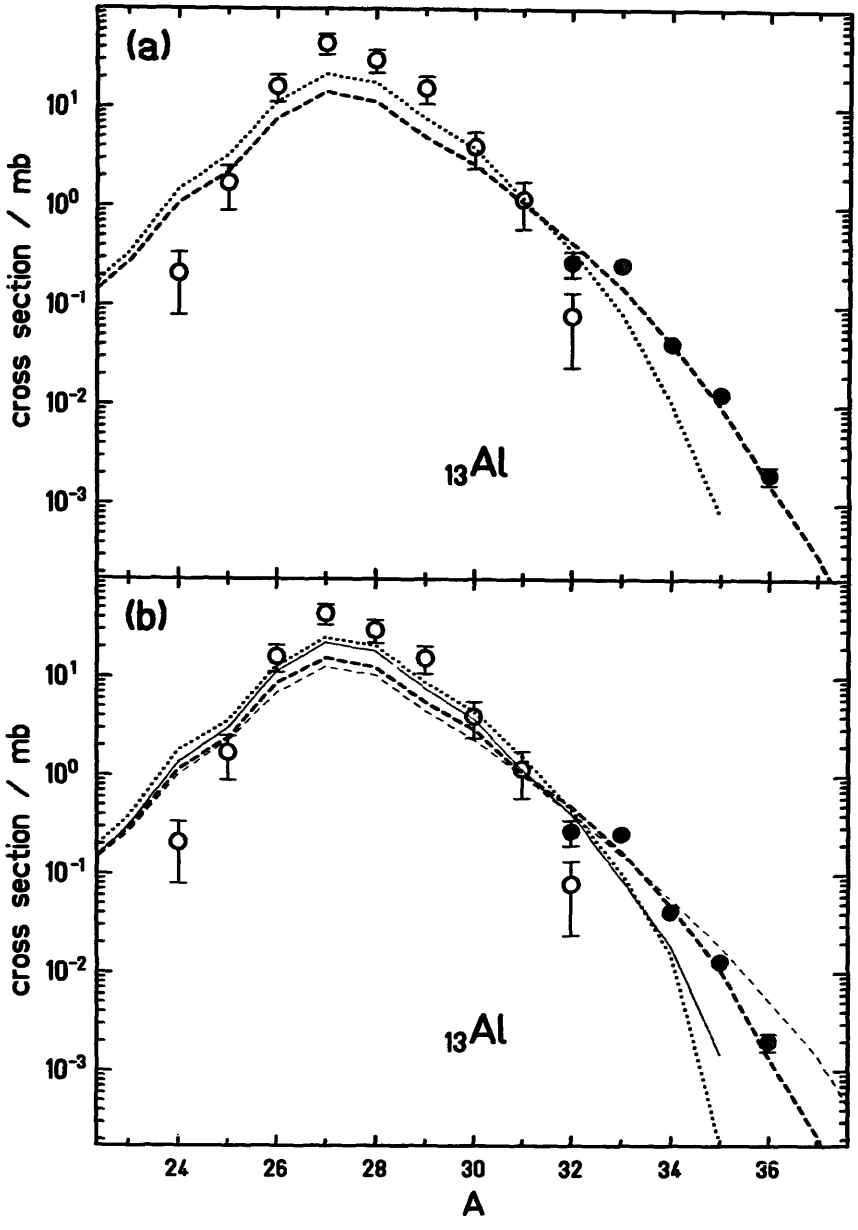

Fig. 13. Cross sections for the production of Al isotopes in different projectile-fragmentation reactions. The points refer to experimental data (see fig. 12). The curves correspond to calculations as explained in fig. 11.

In the following we will use the hypergeometrical model and the statistical hole-energy model for the fragmentation calculations.

4.3. MICROSCOPIC STRUCTURES

In our fragmentation model the microscopic corrections are introduced in the state-density factor of the evaporation model. These corrections enter in two places, in the minimum particle-emission thresholds of the final nucleus by means of the masses and in the state density. When the thresholds are calculated from the

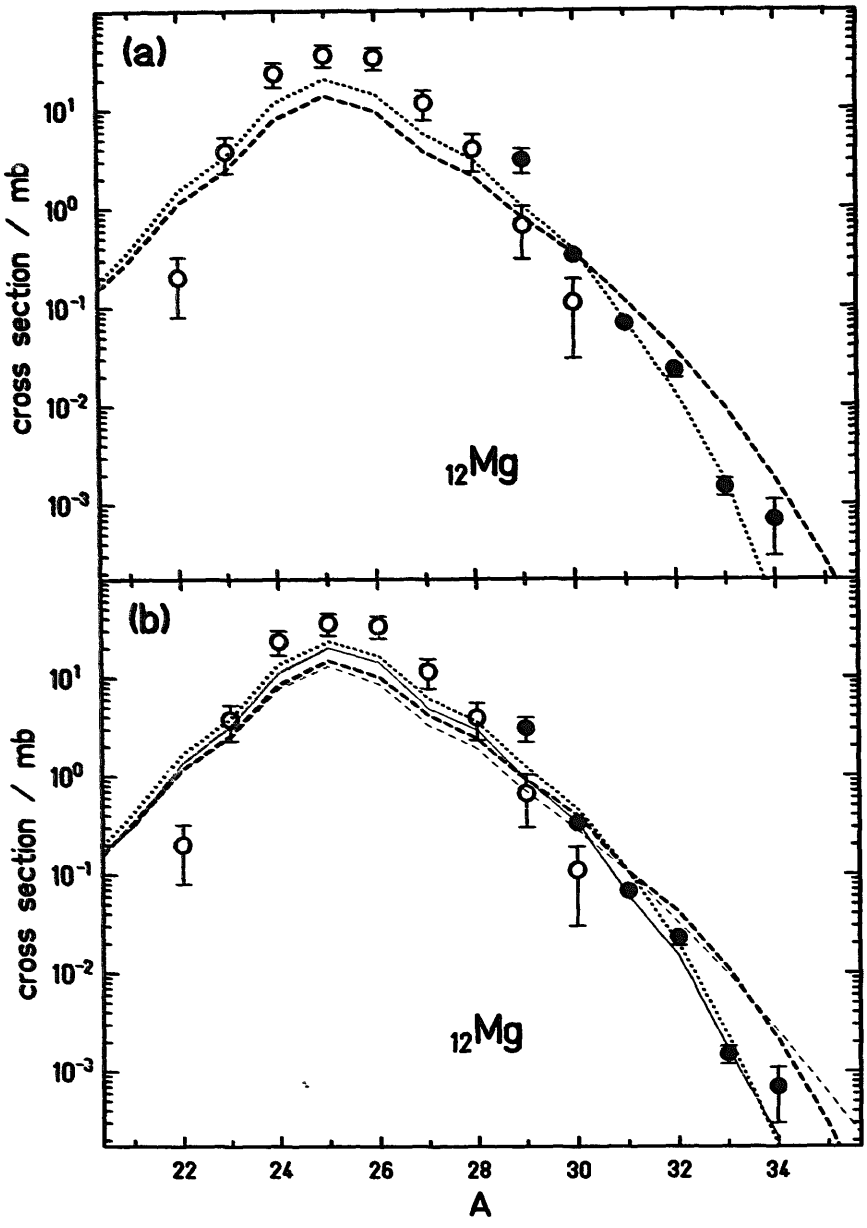

Fig. 14. Cross sections for the production of Mg isotopes in different projectile-fragmentation reactions. The points refer to experimental data (see fig. 12). The curves correspond to calculations as explained in fig. 11.

ground-state masses, an upper limit for the expected pairing structure is obtained because we showed that the pairing structure is reduced when binding energies corresponding to higher angular momenta are used which are more realistic. Fig. 17 shows the calculations with and without microscopic corrections of the isobaric cross sections with mass number 44 and 43 as produced from ^{56}Fe on ^{12}C. The cross-section distribution of even-mass isobars calculated with microscopic corrections is narrower than that without microscopic corrections but it does not show any pairing structure. In contrast to this, the odd-mass isobaric cross sections calculated with the microscopic corrections show a very pronounced pairing struc-

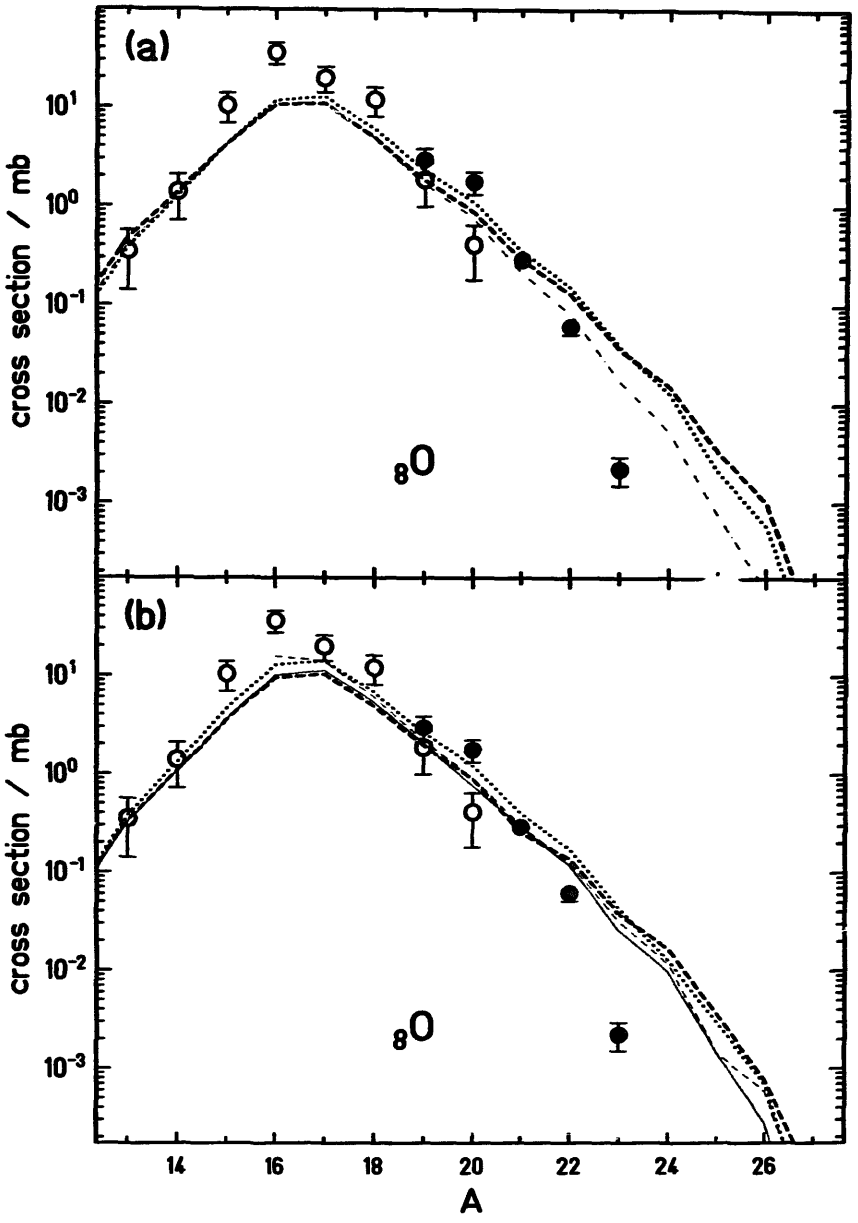

Fig. 15. Cross sections for the production of O isotopes in different projectile-fragmentation reactions. The points refer to experimental data (see fig. 12). The curves correspond to calculations as explained in fig. 11.

ture. This structure is mostly generated by the odd-even structure in the minimum threshold energy. The separation energy S is defined by the mass excesses ΔM:

$$S = [\Delta M_{\text{daughter}} + \Delta M_{\text{emitted particle}}] - \Delta M_{\text{mother}} . \tag{4.1}$$

The state density of the mother nucleus compensates to a great part for the odd-even structure in the mass of the mother. The odd-even structure in the calculated cross sections results nearly completely from the odd-even structure in the mass of the daughter nuclei related to the emission of the most loosely bound particle which is in most cases either a proton or a neutron. This is why the calculated cross sections nearly show no structure for even-mass isobars, the daughter nuclei of which are

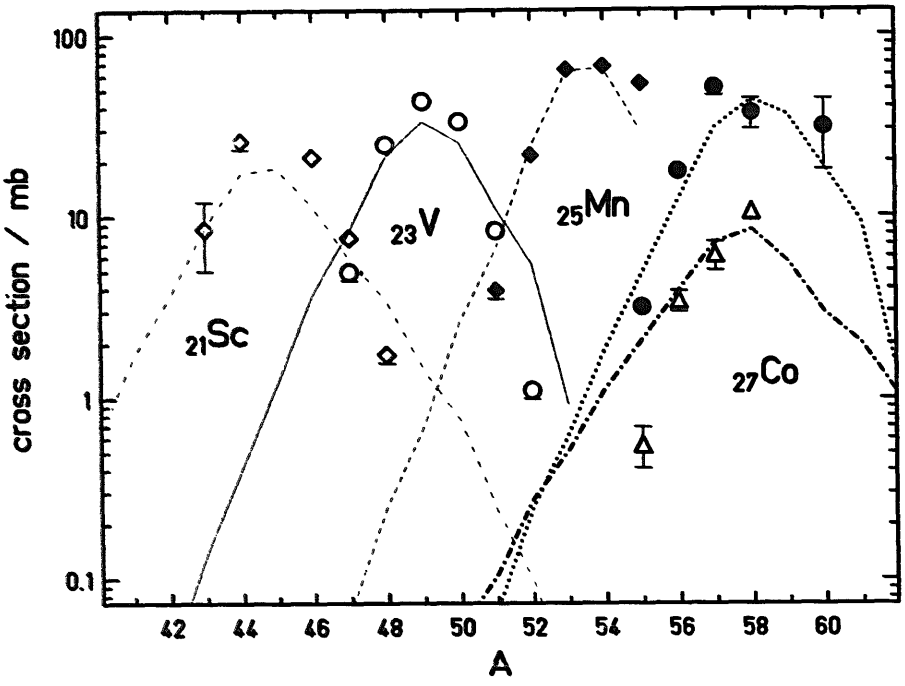

Fig. 16. Comparison of experimental and calculated isotopic cross sections obtained in fragmentation reactions for different elements as indicated in the figure. Open rhombs and full points: target fragmentation in the reaction $^{40}Ar+^{64}Cu$ at 2 GeV/u [ref. [88])]. Open points and full rhombs: projectile fragmentation in the reaction $^{56}Fe+^{12}C$ at 600 MeV/u [ref. [85])]. Open triangles: target fragmentation in the reaction $^{12}C+^{108}Ag$ at 2.1 GeV/u [ref. [89])]. The curves are the result of calculations for these different systems with our fragmentation model: The charge distribution of the prefragments is given by the hypergeometrical model and their excitation energy by the diabatic single-particle vacancy model (this work). The evaporation process is calculated with the modified macroscopic evaporation model (this work).

even-odd or odd-even, but they show a pronounced structure for even-mass isobars, the daughter nuclei of which are even-even or odd-odd. Moreover, the odd-even structure in the cross sections is reversed depending on whether the isobars are neutron rich or proton rich, that means whether they emit predominantly neutrons or protons.

In the fig. 18, the calculated isotopic distributions are compared to experimental results for the elements Au, Al and Mg produced in the fragmentation of ^{209}Bi on ^{12}C and ^{48}Ca on ^{9}Be, respectively. The almost perfect agreement between the experimental cross sections of the most neutron-rich Au isotopes and the calculation with the microscopic effects included is striking. However, the data points of this chemical experiment [84]) for isotopes from ^{190}Au to ^{193}Au and for ^{195}Au are strongly corrected for accumulated activities [90]) and seem to be less reliable with respect to a possible structure effect. The structure in the experimental cross sections of Al and Mg isotopes is much less pronounced than that of the model calculation.

This discrepancy between the predicted and the observed odd-even structure in the cross sections of light fragments may be explained by the fact that the angular momentum of the prefragments was disregarded in our calculation. It was shown in sect. 3.4 that an increased angular momentum tends to reduce the influence of

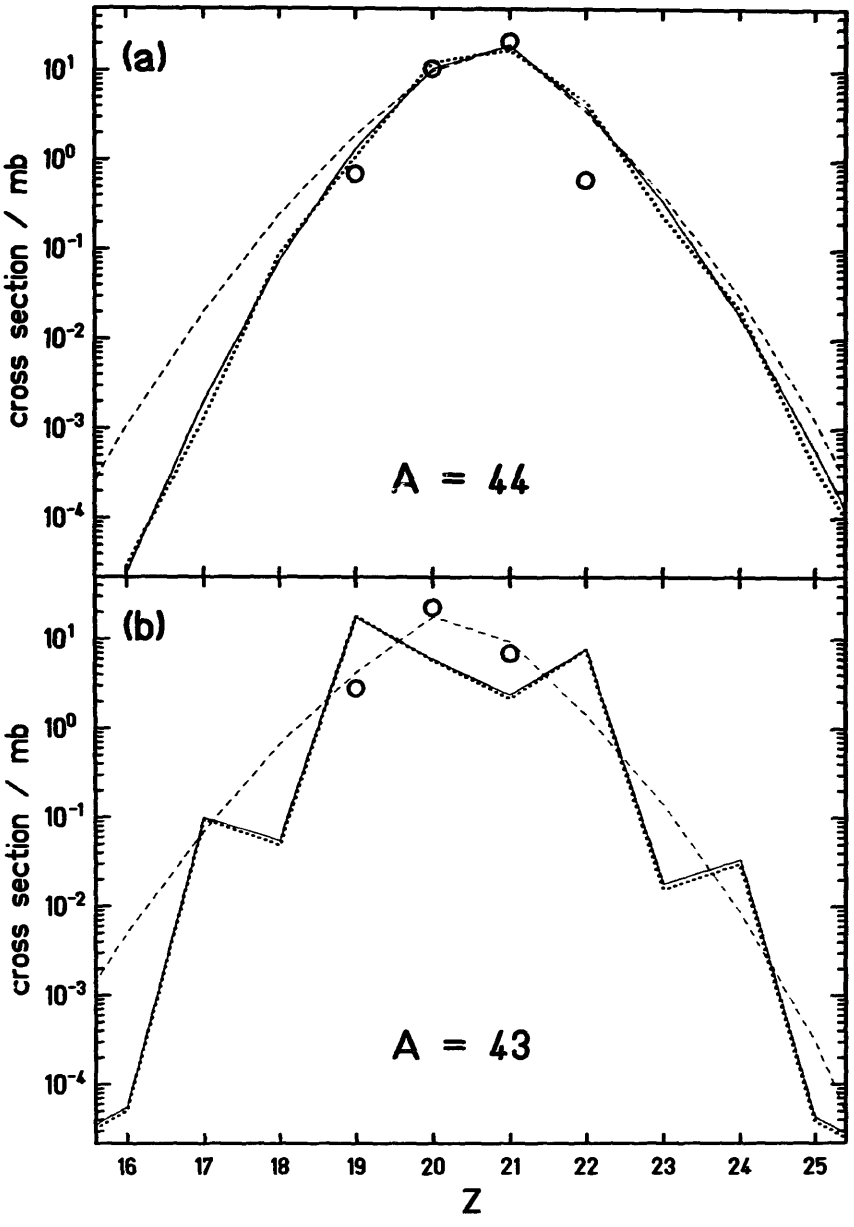

Fig. 17. Isobaric cross sections for $A=44$ (a) and $A=43$ (b) in the reaction $^{56}Fe+^{12}C$ at 600 MeV/u. The data points are taken from ref. [85]). The curves are calculated with our fragmentation model as described in the caption of fig. 16. Different options for the introduction of microscopic effects are used: Dashed lines: no microscopic effects considered. Full lines: shell and pairing corrections introduced in the masses [41,42]) and the level densities [67,68]). Dotted lines: additional inclusion of pairing fine structure (this work).

odd-even structure on the binding energies and hence on the particle thresholds. Moreover, the emission of gamma rays was not considered in our calculations, which might become competitive to the evaporation of particles near the minimum threshold energy. In this way the role of the isolated ground state with its extreme structural influence would be reduced even further.

According to our preceding considerations we do not expect any odd-even structure in the cross sections of even-mass nuclei. However, the production of

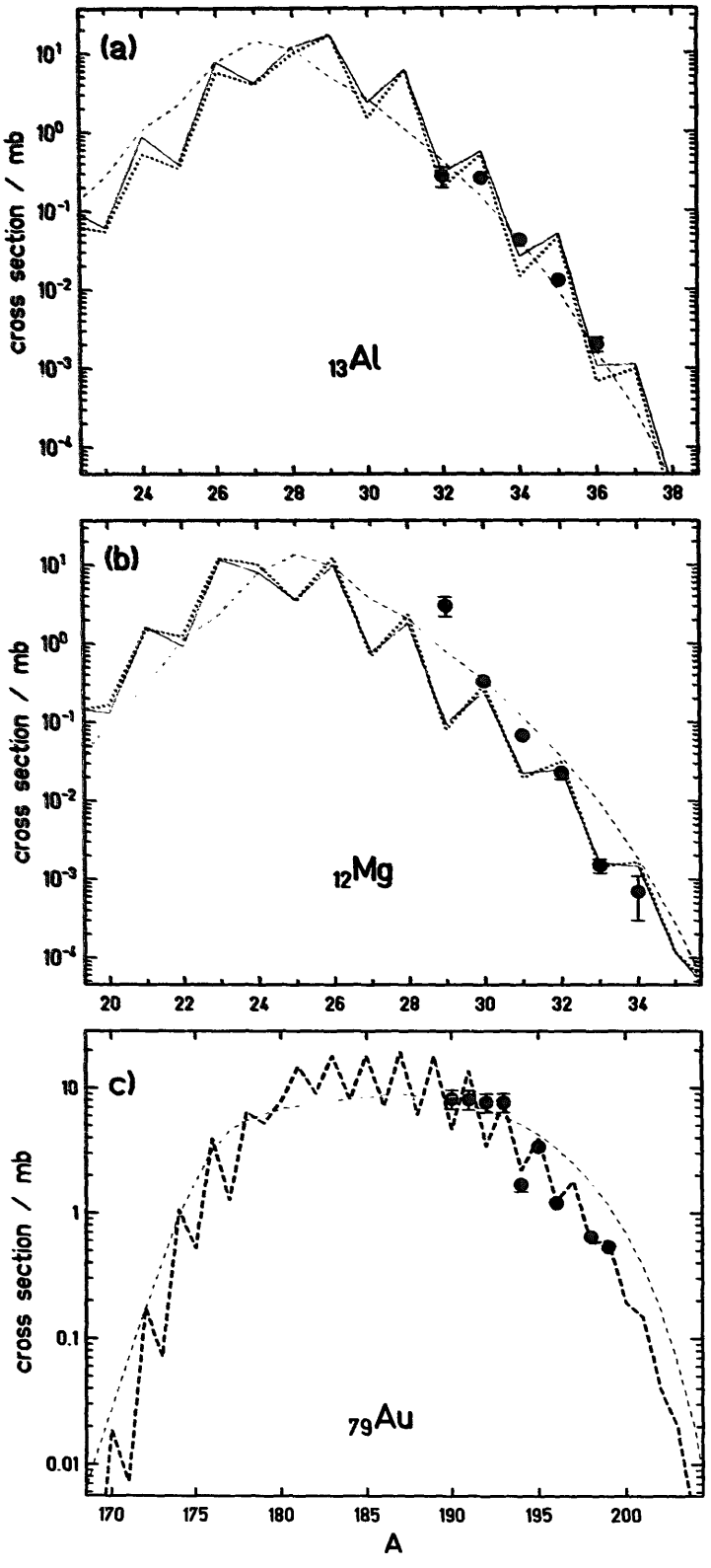

Fig. 18. Production cross sections for Al (a) and Mg isotopes (b) produced as projectile fragments in the reaction ^{48}Ca+^{9}Be at 212 MeV/u and Au isotopes (c) produced as target fragments in the reaction ^{12}C+^{209}Bi at 400 MeV/u. The data are taken from refs. [87,84]). The curves are calculated with our fragmentation model as defined in the caption of fig. 16. Different options for the introduction of microscopic effects are used: In (a) and (b): Dashed lines: no microscopic effects considered. Full lines: pairing corrections introduced in the masses [41,42]) and the level densities [67,68]). Dotted lines: additional inclusion of pairing fine structure (this work). In (c): Thin dashed line: shell corrections introduced in the masses [41,42]) and the level densities [67,68]). Thick dashed line: Shell and pairing corrections introduced in the masses [41,42]) and in the level densities [67,68]), including the pairing fine structure (this work).

nuclei with $A/Z=2$ by the fragmentation of ^{40}Ar by a ^{12}C target showed a distinct enhancement of even-even with respect to odd-odd nuclei [91]). The odd-even structure in these data as defined by

$$R(A,Z)=1-\frac{f(A-2,Z-1)+f(A+2,Z+1)}{2f(A,Z)} \tag{4.2}$$

is shown in fig. 19, with $f(A,Z)$ being the intensity of the nucleus (A,Z). This effect can already be seen in the data of ref. [86]). Also the structure of measured cross sections of nuclei with $A=2Z+2$ from ref. [85]) as well as the predictions of some model calculations are included in the figure. The experimental data are reproduced only when the pairing fine structure, as parametrized by the term δ'', is included in the calculation of the nuclear level density. The variation of the strength of the odd-even structure is reproduced on the average by the model due to the $A^{-1.1}$ dependence in δ''. In this way we demonstrate, on the one hand, the important role of the phase space of the final products for the magnitude of their production cross sections. On the other hand, the observed structure is an interesting source of experimental information on fine structures in the nuclear level density around the threshold energy which is about 10 MeV for these light nuclei.

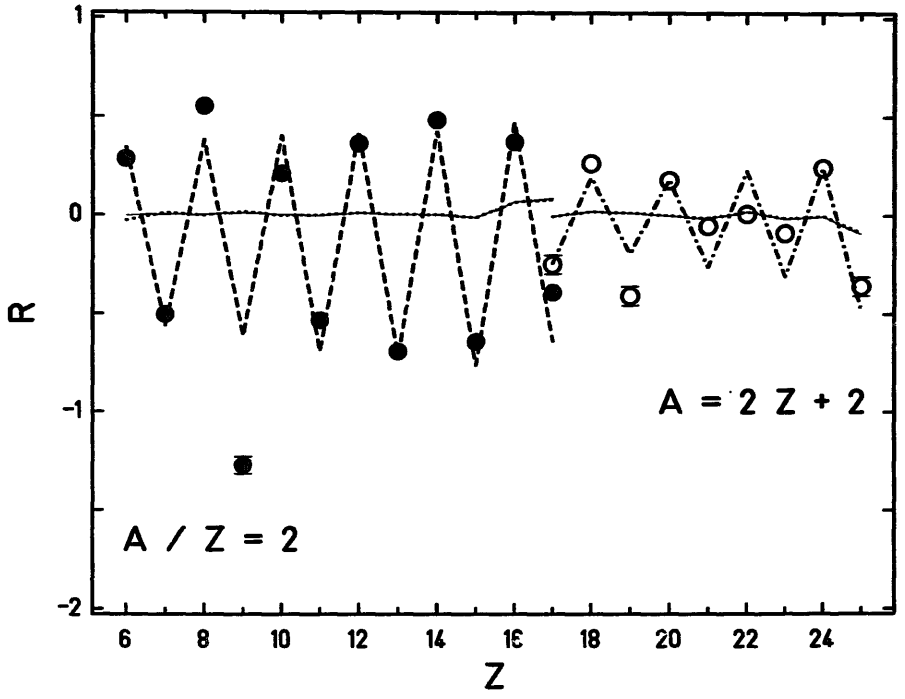

Fig. 19. Odd-even structure in the fragmentation cross sections of light even-mass fragments expressed by the structure parameter R as defined by eq. (4.2). Full points: structure parameter of nuclei with $A/Z=2$ produced in the fragmentation of ^{40}Ar+^{12}C at 403 MeV/u [ref. [91])]. Open points: structure parameter of nuclei with $A=2Z+2$ produced in the fragmentation of ^{56}Fe+^{12}C at 600 MeV/u [ref. [85])]. The curves are calculated with our fragmentation model as defined in the caption of fig. 16. Different options for the microscopic effects are used: Full lines: no microscopic effects included. Dotted lines: pairing corrections introduced in the masses [41,42]) and in the level densities [68]). These curves fall almost together with the full lines. Dashed line and dash-dotted line: additional inclusion of pairing fine structure (this work).

According to the BCS model [69,70]), any influence of pairing correlations on the level densities is expected to vanish above the phase transition at the critical energy. Moreover, systematic structural effects between even and odd nuclei were expected [68]) to show up only in the very lowest levels. Fig. 4a proves that an important odd-even fine structure persists even up to about 10 MeV for these light nuclei. We may expect that part of this structure even persists at appreciably higher excitation energies because microscopic calculations showed that the phase transition between the superfluid and the normal phase is not sharp in a nucleus as a finite even rather small system [71,72]).

5. Conclusion

This work describes a study on nuclear fragmentation, a process occurring in peripheral nucleus-nucleus collisions at relativistic energies. In particular we considered the spectator zones of projectile and target, that means the parts outside the overlap region which finally develop to the projectile and target fragments. For a transparent description of the fragmentation process we chose the geometrical abrasion model for the first stage and the analytical evaporation model of Campi and Hüfner for the second stage of the fragmentation process. After having reexamined these models we propose some improvements and the elimination of some inconsistencies, especially in the calculation of the excitation energies and the angular momenta of the prefragments, in the description of the diffusion process of the evaporation stage and in the treatment of microscopic structures.

While the original abrasion model relates the excitation energy of the prefragments to the surface excess, thus corresponding to an adiabatic process, we propose a diabatic model which deduces the excitation energy from the energy of the vacancies created in the single-particle levels with respect to the Fermi surface. The angular momentum of the prefragment is estimated by a statistical model, similar to that of Goldhaber for the linear momentum, although the angular momentum is not treated explicitly in the present version of the abrasion model. The description of the diffusion process in the evaporation model of Campi and Hüfner was improved by including the statistical weights of the residual states for the emission probabilities of the different particles. The microscopic structures due to pairing correlations and shell effects are introduced in the masses and in the level densities in a consistent way.

Our model reproduces the body of experimental fragmentation cross sections available at this time in a satisfactory way without any adjustable parameter. With the excitation energy calculated from the single-particle vacancies, the yields of light and heavy fragments can be reproduced simultaneously without introducing any additional friction effects. This finding suggests that the contribution of these final-state interactions to the excitation energy of the prefragments is rather weak. The modified evaporation model proved to be in better agreement to elaborated statistical-model calculations than the original one. The weakness of an even-odd

structure in the experimentally observed isotopic yields which is related to the particle thresholds is attributed to angular momentum effects and the competition of gamma emission in the evaporation process. A pronounced even-odd effect in the fragmentation cross sections of light even-mass nuclei could be explained by a fine structure in the level densities around 10 MeV.

This paper is dedicated to P. Armbruster on the occasion of his 60th birthday.

Fruitful discussions with X. Campi, J. Hüfner and W. Nörenberg are gratefully acknowledged. The empirical treatment of the pairing fine structure in the level density was introduced according to a suggestion of A.V. Ignatyuk. We thank H.-G. Clerc for a careful reading of the manuscript. This work has been funded by the German Federal Minister for Research and Technology (BMFT) under the contract number 06DA102I.

References

1) N. Metropolis, R. Bivins, M. Storm, A. Turkevich, J.M. Miller and G. Friedlander, Phys. Rev. **110** (1958) 185, 204
2) J.D. Bowman, W.J. Swiatecki and C.E. Tsang, Lawrence Berkeley Laboratory report LBL-2908 (1973)
3) G. Rudstam, Z. Naturforsch. **A21** (1966) 1027
4) K. Sümmerer and D.J. Morrissey, Proc. First Int. Conf. on Radioactive nuclear beams, Berkeley, 1989, ed. W.D. Myers, J.M. Nitschke and E.B. Norman (World Scientific, Singapore, 1990), p. 122
5) R. Serber, Phys. Rev. **72** (1947) 1114
6) X. Campi, J. of Phys. **A19** (1986) L917
7) J. Nemeth, M. Barranco, J. Desbois and C. Ngô, Z. Phys. **A325** (1986) 347
8) X.-Z. Zhang, D.H.E. Gross, S.-Y. Xu and Y.-M. Zheng, Nucl. Phys. **A461** (1987) 641, 668
9) H.W. Barz, J. Bondorf, R. Donangelo, J.A. Lopez and H. Schulz, Phys. Lett. **B194** (1987) 459
10) S.E. Koonin and J. Randrup, Nucl. Phys. **A471** (1987) 355c
11) W.A. Friedman and W.G. Lynch, Phys. Rev. **C28** (1983) 10
12) W.A. Friedman, Phys. Rev. Lett. **60** (1988) 2125
13) L.G. Moretto and G.J. Wozniak, Nucl. Phys. **A488** (1988) 337c
14) J. Aichelin and G. Bertsch, Phys. Rev. **C13** (1985) 1730
15) H. Kruse, B.V. Jacak and H. Stöcker, Phys. Rev. Lett. **54** (1985) 289
16) R.J. Glauber and G. Matthiae, Nucl. Phys. **B21** (1970) 135
17) J. Hüfner, K. Schäfer and B. Schürmann, Phys. Rev. **C12** (1975) 1888
18) X. Campi and J. Hüfner, Phys. Rev. **C24** (1981) 2199
19) G.D. Westfall, J. Gosset, P.J. Johansen, A.M. Poskanzer, W.G. Meyer, H.H. Gutbrod, A. Sandoval and R. Stock, Phys. Rev. Lett. **37** (1976) 1202
20) W.D. Myers, Nucl. Phys. **A296** (1978) 177
21) D.J. Morrissey, W.R. Marsh, R.J. Otto, W. L[illegible]nd and G.T. Seaborg, Phys. Rev. **C18** (1978) 1267
22) L.F. Oliveira, R. Donangelo and J.O. Ras[illegible]n, Phys. Rev. **C19** (1979) 826
23) W.J. Swiatecki, 1976, unpublished
24) J. Gosset, H.H. Gutbrod, W.G. Meyer, A.M. Poskanzer, A. Sandoval, R. Stock and G.D. Westfall, Phys. Rev. **C16** (1977) 629
25) W.D. Myers and K.-H. Schmidt, Nucl. Phys. **A410** (1983) 61
26) W.D. Myers and W.J. Swiatecki, Ann. of Phys. **84** (1974) 186
27) J.P. Bondorf, G. Fai and O.B. Nielsen, Phys. Rev. Lett. **41** (1978) 391
28) J.W. Wilson, L.W. Townsend and F.F. Badavi, Nucl. Instr. Meth. **B18** (1987) 225
29) A.A. Ross, H. Mark and R.D. Lawson, Phys. Rev. **102** (1956) 1613

30) K.-H. Schmidt, H. Delagrange, J.P. Dufour, N. Cârjan and A. Fleury, Z. Phys. **A308** (1982) 215
31) G. Bertsch, Z. Phys. **A289** (1978) 103
32) W. Nörenberg, Nucl. Phys. **A482** (1988) 221c
33) A.S. Goldhaber, Phys. Lett. **B53** (1974) 306
34) A. Abul-Magd, J. Hüfner and B. Schürmann, Phys. Lett. **B60** (1976) 327
35) W.A. Friedman, Phys. Rev. **C27** (1983) 569
36) B.L. Cohen, Concepts of nuclear physics, ed. T. McGraw-Hill (McGraw-Hill, New Delhi, 1973) p. 74
37) K. Asahi, M. Ishihara, T. Ichihara, M. Fukuda, T. Kubo, Y. Gono, A.C. Mueller, R. Anne, D. Bazin, D. Guillemaud-Mueller, R. Bimbot, W.D. Schmidt-Ott and J. Kagasi, Institute of physical and chemical research report RIKEN-AF-NP-86 (1990)
38) K. Asahi, M. Ishihara, N. Inabe, T. Ichihara, T. Kubo, M. Adachi, H. Takanashi, M. Kouguchi, M. Fukuda, D. Mikolas, D.J. Morrissey, D. Beaumel, T. Shimoda, H. Miyatake and N. Takahashi, Institute of physical and chemical research report RIKEN-AF-NP-87 (1990)
39) U. Gollerthan and K.-H. Schmidt, Gesellschaft für Schwerionenforschung report GSI-86-1 (1986) p. 63
40) A.H. Wapstra and G. Audi, Nucl. Phys. **A432** (1985) 1
41) W.D. Myers and W.J. Swiatecki, Nucl. Phys. **81** (1966) 1
42) W.D. Myers and W.J. Swiatecki, Proc. Int. Symp. on Nuclides far off the stability line, Lysekil, 1966, ed. W. Forsling, C.J. Herrlander and H. Ryde (Almqvist and Wiksell Boktryckeri, Uppsala, 1967) p. 343
43) P.M. Endt and C. van der Leun, Nucl. Phys. **A310** (1978) 1
44) F. Ajzenberg-Selove, Nucl. Phys. **A392** (1983) 1, 120
45) F. Ajzenberg-Selove, Nucl. Phys. **A433** (1985) 43
46) F. Ajzenberg-Selove, Nucl. Phys. **A449** (1986) 53
47) F. Ajzenberg-Selove, Nucl. Phys. **A460** (1986) 1
48) D.C. Kocher, Nucl. Data Sheets **11** (1974) 279
49) H.W. Müller and J.W. Tepel, Nucl. Data Sheets **27** (1979) 339
50) P. Luksch, Nucl. Data Sheets **30** (1980) 573
51) B. Singh and D.A. Viggars, Nucl. Data Sheets **33** (1981) 189
52) P. De Gelder, D. de Frenne and E. Jacobs, Nucl. Data Sheets **35** (1982) 443
53) H.W. Müller, Nucl. Data Sheets **35** (1982) 281
54) B. Singh and D.A. Viggars, Nucl. Data Sheets **36** (1982) 127
55) H.W. Müller, Nucl. Data Sheets **39** (1983) 467
56) J. Blachot, J.P. Husson, J. Oms and G. Berrier, Nucl. Data Sheets **41** (1984) 325
57) B. Singh and D.A. Viggars, Nucl. Data Sheets **42** (1984) 233
58) H.W. Müller, Nucl. Data Sheets **44** (1985) 277
59) H.W. Müller, Nucl. Data Sheets **50** (1987) 1
60) B. Singh and D.A. Viggars, Nucl. Data Sheets **51** (1987) 225
61) H.W. Müller and J.W. Tepel, Nucl. Data Sheets **54** (1988) 527
62) B. Singh and D.A. Viggars, Phys. Rev. **29** (1980) 75
63) B. Singh and D.A. Viggars, Nucl. Data Sheets **37** (1982) 393
64) J. Müller, Nucl. Data Sheets **46** (1985) 487
65) J.R. Huizenga and L.G. Moretto, Annu. Rev. Nucl. Sci. **22** (1972) 427
66) L.G. Moretto, Proc. Third IAEA Symp. on the physics and chemistry of fission, Rochester, 1973 (International Atomic Energy Agency, Vienna, 1974) vol. 1, p. 329
67) A.V. Ignatyuk, G.N. Smirenkin and A.S. Tiskin, Yad. Fiz. **21** (1975) 485 (Sov. J. Nucl. Phys. **21** (1975) 255)
68) A.V. Ignatyuk, K.K. Istekov and G.N. Smirenkin, Yad. Fiz. **29** (1979) 875 (Sov. J. Nucl. Phys. **29** (1979) 450)
69) J. Bardeen, L.N. Cooper and J.R. Schrieffer, Phys. Rev. **108** (1957) 1157
70) A. Bohr, B.R. Mottelson and D. Pines, Phys. Rev. **110** (1958) 936
71) A.V. Ignatyuk and Yu.V. Sokolov, Yad. Fiz. **19** (1974) 1229 (Sov. J. Nucl. Phys. **19** (1974) 628)
72) J.L. Egido, P. Ring, S. Iwasaki and H.J. Mang, Phys. Lett. **B154** (1985) 1
73) A.V. Ignatyuk, private communication

74) J. Töke and W.J. Swiatecki, Nucl. Phys. **A372** (1981) 141
75) M.K. Grossjean and H. Feldmeier, Nucl. Phys. **A444** (1985) 113
76) A.V. Ignatyuk, M.G. Itkis, V.N. Okolovich, G.R. Rus'kina, G.N. Smirenkin and A.S. Tishin, Yad. Fiz. **25** (1977) 25 (Sov. J. Nucl. Phys. **25** (1977) 13)
77) B. Harmatz, Nucl. Data Sheets **22** (1977) 433
78) B. Harmatz, Nucl. Data Sheets **23** (1978) 607
79) J. Halperin, Nucl. Data Sheets **28** (1979) 485
80) E. Browne, Nucl. Data Sheets **30** (1980) 653
81) V.S. Shirley, Nucl. Data Sheets **32** (1981) 593
82) V.S. Shirley and J.M. Dairiki, Nucl. Data Sheets **40** (1983) 425
83) J.-J. Gaimard, Ph.D. thesis, Université Paris 7 (1990)
84) K. Aleklett, D.J. Morrissey, W. Loveland, P.L. McGaughey and G.T. Seaborg, Phys. Rev. **C23** (1981) 1044
85) W.R. Webber, J.C. Kish and D.A. Schrier, Phys. Rev. **C41** (1990) 547
86) Y.P. Viyogi, T.J.M. Symons, P. Doll, D.E. Greiner, H.H. Heckman, D.L. Hendrie, P.J. Lindstrom, J. Mahoney, D.K. Scott, K. van Bibber, G.D. Westfall, H. Wieman, H.J. Crawford, C. McParland and C.K. Gelbke, Phys. Rev. Lett. **42** (1979) 33
87) G.D. Westfall, T.J.M. Symons, D.E. Greiner, H.H. Heckman, P.J. Lindstrom, J. Mahoney, A.C. Shotter, D.K. Scott, H.J. Crawford, C. McParland, T.C. Awes, C.K. Gelbke and J.M. Kidd, Phys. Rev. Lett. **43** (1979) 1859
88) J.B. Cumming, P.E. Haustein, T.J. Ruth and G.J. Virtes, Phys. Rev. **C17** (1978) 1632
89) N.T. Porile, G.D. Cole and C.R. Rudy, Phys. Rev. **C19** (1979) 2288
90) D.J. Morrissey, D. Lee, R.J. Otto and G.T. Seaborg, Nucl. Instr. Meth. **158** (1979) 499
91) B. Blank, J.-J. Gaimard, H. Geissel, G. Münzenberg, K.-H. Schmidt, H. Stelzer, K. Sümmerer, H.-G. Clerc, E. Hanelt, B. Voss, D. Bazin, R. Del Moral, J.-P. Dufour, A. Fleury and M.S. Pravikoff, Nucl. Instr. Meth. **A286** (1990) 160